8-2020

Development of Plant Extract-Based Composite Fibers and Aerogels

Raul C. Barbosa
The University of Texas Rio Grande Valley

DEVELOPMENT OF PLANT EXTRACT-BASED COMPOSITE FIBERS AND AEROGELS

A thesis

by

RAUL C. BARBOSA

Submitted to the Graduate College of
The University of Texas Rio Grande Valley
In partial fulfillment of the requirements for the degree of

MASTER OF SCIENCE IN ENGINEERING

August 2020

Major Subject: Mechanical Engineering

DEVELOPMENT OF PLANT EXTRACT-BASED

COMPOSITE FIBERS AND AEROGELS

A thesis
by
RAUL C. BARBOSA

COMMITTEE MEMBERS

Dr. Karen Lozano
Chair of Committee

Dr. Victoria Padilla
Committee Member

Dr. Javier Ortega
Committee Member

Dr. Rogelio Benitez
Committee Member

August 2020

ABSTRACT

Barbosa, Raul C, Development of Plant Extract-Based Composite Fibers and Aerogels. Master of Science Engineering (MSE), August 2020, 81 pp; 37 figures, 188 references.

The aim of this study is to use the solid templating process of pullulan nanofibers in order to produce biocompatible, biodegradable, and antibacterial aerogels. The developed aerogels were produced using cross-linked pullulan nanofibers, which provide a water-stable structure allowing them to be used as wound dressing material. The morphology, thermal properties, water solubility, and thermal and physical properties of the nanofibers and aerogels were characterized. Furthermore, the antibacterial effect against gram-negative bacteria, Escherichia coli, and the biocompatibility using mouse embryonic fibroblasts (NIH 3T3) were investigated.

DEDICATION

I want to dedicate this work to my parents, Dalilia Mendoza and Raul Barbosa, who have always showed me love, encouragement, and support; my wife, Amanda Pena, for her comprehension, support, and love; also, my siblings: Aleida, Maximiliano, Leonardo, and Emiliano for their love and affection. Thanks to you I have become the person I am today.

ACKNOWLEDGMENTS

I would like to express my appreciation to Dr. Karen Lozano for her guidance, support, and encouragement. Her attitude and ability towards achieving goals have inspired me to become a better student and person.

I would also like to thank Dr. Javier Ortega and Dr. Rogelio Benitez for their support and counseling, as well as Dr. Victoria Padilla, for helping me analyze my experiments and results in depth. Last but not least, I would like to thank my lab partners Carlos, Ydana, Dulce, Misael, Heriberto, and Alexa for helping me throughout my projects.

This project is supported by the NSF PREM award under grant No. DMR-1523577: UTRGV-UMN Partnership for Fostering Innovation by Bridging Excellence in Research and Student Success.

TABLE OF CONTENTS

Page

LIST OF FIGURES

Page

CHAPTER I

INTRODUCTION

Wound healing is a normal biological response in the human body achieved through four sequential phases: hemostasis, inflammation, proliferation, and remodeling. Effective and efficient wound healing is possible through harmonious and timely achievement of the aforementioned phases. However, there are many factors that can adversely affect this process, which may lead to chronic wounds and improper tissue repair. Wounds that failed to properly proceed through the normal stages of healing, or in the expected amount of time, are considered chronic wounds. These types of wounds result in a delayed or incomplete healing process which can cause significant burden to the patients, healthcare system, and society.

A wide variety of innovative wound dressings, specifically designed to treat chronic wounds, have been developed in the last years. They typically replace damaged tissue and provide a favorable environment for proper wound healing. Aerogels are one of these special wound dressings. An aerogel is a nanostructured network with open pores, high specific surface area, and porosity of at least 90%. Its three-dimensional structure exhibits extraordinary properties, including absorption of high amounts of exudate, thus, preventing wound infections. They can also be used to incorporate ingredients that facilitate and accelerate the healing cycle.

Polysaccharide-based aerogels for wound healing application have attracted a lot of attention due to their inert nature, biocompatibility, and good chemical and mechanical properties. Enhancement of such aerogels have been obtained with the addition of natural and synthetic ingredients. The aim of this study is to use the solid templating process of pullulan nanofibers, with the addition of aloe vera extract, to produce biocompatible, biodegradable, and non-toxic aerogels which can be used as an alternative or complement to current wound healing methods.

CHAPTER II

REVIEW OF LITERATURE

2.1 Wound Healing Process

Wound healing is a normal biological response in the human body achieved through four sequential phases: hemostasis, inflammation, proliferation, and remodeling [1]. An overview illustrating the normal wound healing phases is presented in Fig. 1. Effective and efficient wound healing is possible through harmonious and timely achievement of the aforementioned phases. However, there are many factors that can adversely affect this process, which may lead to chronic wounds and improper tissue repair [3].

2.1.1 Hemostasis

The normal wound healing process starts with hemostasis, which enables the process of blood clotting, vascular repair, and activation of the platelets. At the injury site, adhesion and aggregation of platelets to the damaged site begin, followed by the generation of thrombin by the exposure of subendothelial tissue factor to the bloodstream. Thrombin converts soluble fibrinogen into fibrin fibers that crosslink near fibrin chains to form a polymerized flexible fibrin clot at the wound site. That clot minimizes blood loss and serves as a scaffold to support initial cellular infiltration and epithelial migration. In addition, the small amount of thrombin enables activation of different coagulation elements and platelets. [1, 3, 4]

TABLE I. Phases of the normal wound-healing process

Phase	Timeframe	Cells involved	Function	Cellular and biophysical events
Haemostasis	Immediate	Platelets (also called thrombocytes and involved in blood clotting)	Clotting	» Vascular constriction » Platelet aggregation, degranulation, and fibrin formation (thrombus)
Inflammation	Day 1-4	» Monocytes » Lymphocytes » Neutrophils » Macrophages	Phagocytosis (ingestion of bacteria)	» Neutrophil infiltration » Monocyte infiltration, and differentiation of macrophages » Lymphocyte infiltration
Proliferation	Day 4-21	» Macrophages » Lymphocytes » Angiocytes » Neutrophils » Fibroblasts » Keratinocytes	» Re-establishment of skin function » Wound bed filling » Wound closure	» Re-epithelialisation » Angiogenesis (growth of new capillaries) » Collagen synthesis
Remodelling	Day 21-year 2	Fibrocytes	» Develop tensile strength	» Collagen remodelling » Vascular maturation and regression

Figure 1. Details about timeframe, cells involved, function, and cellular/biophysical events found in each phase of the normal wound-healing process. [2]

2.1.2 Inflammation

In the inflammation phase, histamine promotes vessel dilation and causes the formation of pores in the blood vessel walls. This allows facile access of necessary cells into the damaged area. Furthermore, the activation of platelets releases growth factors, (e.g. transforming growth factor-beta [TGF-β] and platelet-derived growth factor [PDGF]), which promote proliferation of inflammatory cells such as neutrophils and monocytes, as well as cell migration of fibroblast and vascular endothelial cells. [5] Neutrophils are the first cells to arrive at the wound area and are responsible for removing invading microbes and cellular debris, which helps to prevent infection; they also release cytokines that help attract monocytes. Subsequently, monocytes enter

the wound area and turn into macrophages. Macrophages implement different functions such as perpetuating inflammatory reactions, phagocytosis, and the release of various growth factors. Macrophages phagocytize pathogens, cells and debris, which further help clean and protect the wound from foreign substances and infections. Besides helping to maintain a clean environment within the wound, macrophages release certain growth factors that activate different signals used to coordinate and facilitate the wound healing process. [6,7]

2.1.3 Proliferation

During the proliferation phase, the emergence of new granulation tissue and epidermis begins. Granulation tissue is composed of macrophages, fibroblasts, collagen, new blood vessels, and antibodies which provide support for the new epidermis. The formation of granulation tissue starts by the attraction and proliferation of fibroblasts into the wound as a result of the coordinated release of growth factors by the macrophages. [8] Fibroblasts produce collagen (type III), which is a high tensile strength protein that's formed in strands inside the wound. Additionally, they produce the ground substance, which is an amorphous, gel-like material that fills up the gaps between cells and collagen strands. Once Fibroblasts have produced enough collagen to support further cell migrations, they will differentiate into myofibroblasts due to growth factor stimuli. Myofibroblasts begin linking with each other and use collagen strands to start holding the edges of the wound together thereby starting contraction. Contraction can reduce the wound size by 40% to 80% its original size and can continue contracting after complete re-epithelialization. [9, 10] Macrophages release growth factors (e.g. vascular endothelial growth factor and PDGF) that go into the surrounding blood vessels. This promotes the adjacent vascular endothelial cells to form new blood vessels (angiogenesis) by following a

coordinated series of vascular morphogenic steps. The new blood vessels infiltrate the wound, where they play the vital part of providing oxygen and nutrients. [11,12]

While the granulation tissue is being formed, re-epithelialization of the wound is occurring. Basal keratinocyte cells from the wound margin dissolve the intervening basement membrane and start migrating with minimum proliferation along the edges. As the cells cover the edges of the wound, they start proliferating to provide a viable way to migrate across. This movement of the cells is promoted by nitric oxide as well as the lack of contact inhibition. The keratinocytes migrate underneath the blood clot and over the granulation tissue, depositing basement membrane proteins and growth factors that help in the epithelialization process and in the wound's immune defense. Ultimately, keratinocytes will come from both sides and meet in the midline, causing them to stop due to point contact inhibition. At that point re-epithelialization of the wound will be complete (usually within 48 hours). [13-16]

2.1.4 Remodeling

In the remodeling phase, type III collagen proteins are replaced by type I collagen proteins, which then are reorganized, remodeled, and matured. During this period, disorganized collagen fibers are rearranged, and excess collagen is removed. Absorbance of water from the scar allows collagen fibers to come closer to each other promoting cross-linking of the fibers; thus, increasing the wounds tensile strength. [1,17,18]

During this phase, endothelial cells, myofibroblasts, and macrophages either exit the wound or undergo apoptosis (programmed cell death) while protein synthesis decreases. The remaining components in the wound include collagen, cells, and some extracellular-matrix proteins. [19] As the wound's tensile strength increases, it reaches a maximum strength of 80%

of the original tissue, which is characterized by the evolution of a softer granulation tissue into a strong mature scar. This process continues for weeks and can last months, even years, depending on the severity of the wound. [7,10,20] Many factors can adversely affect the wound healing process and can lead to health complications and chronic wounds.

2.2 Chronic Wounds

Wounds that failed to properly proceed through the normal stages of healing or in the expected amount of time are considered chronic wounds. The main local and systematic factors that can adversely affect the wound healing process include infection, poor blood supply, presence of necrotic tissue, inadequate nutrition, and advanced age. This results in a delayed or incomplete healing process which can cause significant burden to the patients, healthcare system, and society. [21]

Infections develop from the proliferation of pathogenic microorganisms in the wound which give rise to the features of inflammation. [22] Infected wounds may take a longer time to heal, or don't heal at all and become chronic. Infected wounds contain pathogens that release toxins, causing ongoing damage to the tissues and preventing wound healing from taking place. Proper usage of localized wound cleaning treatments and good management can minimize and eliminate the infection thus allowing the wound to heal properly.

Another factor that may cause chronic wounds is necrotic tissue. The presence of necrotic tissue that wasn't removed by macrophages entails negative consequences for different reasons. For example, the necrotic tissues act as a habitat and a source of food for bacteria, which highly increases the chances of developing an infection. [23] Also, living cells need to move over living

cells, so having necrotic tissue prevents cellular migration which results in unsuccessful completion of the wound healing process.

Poor circulation, which results in a minimized blood supply, limits the oxygen and nutrients supplied to the wound and may also result in improper healing. Furthermore, advanced age can contribute to chronic wounds. The ability of aged skin to repair wounds declines over time, making it more susceptible to infections and generating a variety of health complications. This degeneration of the wound healing process is attributed to less efficient keratinocytes. They exhibit reduced proliferation and migration which decreases the efficiency in re-epithelization. [24]

Nutrition is also an important systematic factor affecting wound healing. In order to properly undergo this metabolically demanding process, the energy from carbohydrates is utilized. If enough carbohydrates are not present, the body will start breaking down its protein supply into amino acids in order to use them to produce energy. Carbohydrates are important in preventing excessive muscle break down and in the anabolic process during the proliferative phase; proteins are essential to angiogenesis, fibroblast proliferation, immune function and to build up the new tissues. [25] Deficiency or inadequate basic nutrition can result in a poor immune system and negatively affect the phases of the wound healing process.

Chronic wounds are a current problem that is rising in a correlated manner every year with the increasing incidences of conditions that limit or adversely affect the normal wound healing process. Worldwide chronic wound care has become such a major challenge in the healthcare system, that a specialty treating this condition has been established. [26]

2.3 Chronic Wounds Classifications

Chronic wounds can be classified in three main categories: diabetic ulcers, pressure ulcers, and venous ulcers. There are similar features shared among these wounds, however, the underlying pathologies differ for each one of them. [26]

2.3.1 Diabetic Ulcers

Diabetic foot ulcers (DFUs) are a chronic complication of diabetes that occur as a result of various factors including neuropathy, foot deformity, and peripheral arterial disease (PAD) [27,28] Neuropathy is used to describe disorders affecting the peripheral nerves, which are located outside the brain and spinal cord where they communicate information to and from the rest of the body. PAD is a circulatory problem in which narrowed arteries, due to plaque buildup, reduce the blood flow to organs and other parts of the body (usually the legs). Typically, trauma or abnormal loading of the foot are triggers of DFUs. [29] After the triggering of ulcers or infections in the foot, blood supply needs to be increased in order to take enough nutrients and oxygen to the wound for proper healing. PAD and neuropathy hinder this development, impairing wound healing; thus, resulting in a chronic wound.

Patients with diabetes have an incidence of 1% to 4% annually, and an estimated 25% lifetime risk of developing DFUs. [30] Due to its prevalence and intensity, DFUs are the leading cause of hospitalization when compared to any other diabetic complications, thus, increasing mortality and morbidity in diabetes. [31-33] Moreover, people with DFUs have a high risk of limb loss through amputation, and a 47% increased mortality risk when compared with diabetic individuals without DFUs. [34,35] A study by Brennan, et al. [36] showed that the survival rates of people with DFUs at 1-, 2-, and 5- years were 81, 69, and 29%, respectively, while another

study by Morbach et al. [37] concluded that cumulative mortalities at years 1, 3, 5 and 10 were 15.4%, 33.1%, 45.8%, and 70.4%. Both studies suggest a high mortality and dismal long-term survival rates, where the 5-year mortality rate is similar or worse than many common types of cancer. [38]

In addition to a decline on physical/mental health and quality of life, patients with DFUs usually encounter substantial economic distress due to the cost of everything from interventions to care and management after amputations. [39] Rice et al. [40] estimates that the annual cost of DFUs ranges from $9-13 billion in the United States. The total direct cost for healing ulcers where an amputation is not required is approximately $17,500 and the cost for amputations in lower-extremities is about $30,000-$33,500. [41] In order to improve treatment outcomes (thus, improving economic burden, amputation rates, survival rates, and quality of life), appropriate initiatives, structural changes, and management should be implemented.

2.3.2 Pressure Ulcers

Pressure Ulcers (PUs), also referred to as pressure injuries, decubitus ulcers, or bed sores, are localized areas of the skin or underlying tissue damaged by pressure, friction, shear or a combination thereof. They develop as a consequence of a breakdown of soft tissue due to pressure between an external surface and a bony prominence. [42,43] Up to 70% of all PUs affect the hip and buttock area, where the most common areas are the trochanter, ischial tuberosity, and sacrum. An additional 15-25% occur in the lower extremities, and the rest may develop in locations where long periods of constant pressure is experienced. [44] Elderly and bed-bound individuals have a higher chance of developing PUs due to their limited activity or immobility.

PUs are categorized in four different stages, following the system established by the National Pressure Injury Advisory Panel (NPUAP) [45], which are as follows:

Stage 1: Intact skin with non-blanchable erythema areas

Stage 2: Exposed dermis with partial-thickness skin loss

Stage 3: Full-thickness skin loss

Stage 4: Full-thickness skin and tissue loss

This system doesn't follow a level of progression, instead it classifies the degree of the injury based on the amount of tissue damaged, similar to how burns are categorized. Many PUs arises in hospitals, especially from patients in intensive care where a prevalence of 4%-49% and incidence ranged from 3.8% to 12.4% exist. [46-49] The Agency for Healthcare Quality and Research estimated that PUs affects approximately 2.5 million people and account for 60,000 deaths in the United States. Additionally, it estimates that the cost of PUs per individual patient ranges from $20,900 to $151,400, which can total from $9.1 billion to $11.6 billion per year. [50] The health and financial implications encompassing PUs are substantial; therefore, prevention and mitigation of pressure ulcers through better management practices and research should be of high importance.

2.3.3 Venous Ulcers

Venous ulcers (VUs) are commonly caused by an increase in pressure on the lower leg's venous system. This results from venous valvular obstruction and/or insufficiency in the deep and lower perforating veins. Valves inside the veins are designed to prevent reflux of the pumped blood and help maintain controlled blood pressure. When those valves become ineffective,

venous valvular insufficiency occurs. Over time, the increased pressure on the veins causes capillary and venous circulation problems, resulting in the formation of ulcers. [51]

Valvular incompetence affects up to 10% of the North American and European population, from which 0.2% develop venous ulcerations. [52] The prevalence of VUs increases as people get older, affecting 0.6%-3% of individuals over 60 years of age and over 5% of those older than 80. [53] The economic cost of treating VUs varies between countries; for example, in the US the estimated cost is between $1.9–$14.9 billion, where in the rest of the western hemisphere it's approximately 1% of their entire health care cost. [54-56]

2.4 Advanced Interventions for Chronic Wounds

2.4.1 Negative Pressure Wound Therapy

Negative pressure wound therapy (NPWT) applies negative pressure at the wound bed to create a suction that removes excess fluid, thereby enhancing blood flow and reducing bacterial contamination and edema. During the procedure a dressing (usually a gauze or foam) is placed inside the wound with drainage tubing placed over it. Subsequently, the dressing is covered with a transparent adhesive film to provide an airtight seal. The drain tube then gets connected to a vacuum pump which is programmed to provide intermittent, or continuous pumping, which removes excess fluid from the wound and sends it to a collection canister. This treatment is a relatively non-invasive option that allows patients to receive this therapy from the comfort of their own home. However, some studies indicate that NPWT demonstrates a beneficial effect on wound healing [57,58] while others suggest that the effectiveness to heal wounds is unclear. [59,60]

2.4.2 Electrical Stimulation

Electrical stimulation (ES) involves sending an electric current through electrodes that are placed on or around the wound. There are two methods in which ES can be achieved. The first method involves placing two electrodes with the same polarity on opposite sides of the wound and a third electrode with opposite polarity nearby the wound. In the second method, one electrode is placed on a sterile, conductive material that's on the wound while the other electrode is placed close to the wound on intact dry skin. [61] It is suggested that ES can accelerate or restart wound repair by imitating the natural electrical current that occurs in injured skin, moreover, it can reduce infection, improve cellular immunity, and increase cutaneous wound healing. [62,63] This method has shown positive results without any adverse effects, indicating that this therapy is safe to use. Nonetheless, further research is required in order to understand how to optimize timing and doses, which type of ES should be applied, and which are appropriate applications.

2.4.3 Ultrasound

Ultrasound (US) therapy uses sound waves to produce heat within the tissue in order to help treat different soft tissue injuries. This procedure is usually separated into two classes: low and high intensity. The procedure consists of using an US probe covered with a conducting gel, which is then used to massage the affected area delivering the frequency required. When applied correctly, US can accelerate the initial inflammatory phase during wound healing, as well as enhance the collagen synthesis by fibroblast. [64] Furthermore, treated scar tissue may result stronger and more elastic than non-treated scars. [65] Disadvantages of US treatments include burns or damage to the endothelial, inactivate or altered enzymes, and conflicting clinical evidence about its effectiveness. [66,67]

2.4.4 Larval Therapy

Larval therapy, also known as maggot therapy, employs sterile larvae to perform selective debridement of the wound. This involves placing larvae on the wound surface, in a mesh pouch or free range, and allow them to remove necrotic tissue through two mechanisms. One, the larvae releases proteolytic enzymes that soften and decompose necrotic tissue without harming the healthy tissue. Two, they can also dissolve necrotic tissue, and subsequently ingest it along with bacteria (including antibiotic resistant strains). This larval therapy provides debridement, disinfection, and enhancement of wound healing, and has become an invaluable tool in treating chronic wounds. [68] Despite the benefits of larval therapy, apprehension from patients and medical staff, as well as the itching and irritating tickling sensation might cause reluctance to adopt this treatment. [69]

2.4.5 Wound Dressings

There are several innovative wound dressings that are specifically designed to treat chronic wounds. They typically replace damaged tissue and provide a favorable environment for proper wound healing. These dressings can be made out of biocompatible polymers and contain a variety of materials including antibacterial agents and cell growth factors. Dressing examples include dry, wet-to-dry, hydrogel, foam, and bioactive dressings. Dry dressings include traditional gauze pads and bandages. They are permeable, inexpensive, nonocclusive, and provide protection to the wound from bacteria and injury in addition to assisting with the healing process. Wet-to-dry dressings are semipermeable films, or moist gauzes, which allow for removal of wound debris and necrotic tissue when the dressing is removed. Hydrogel dressings are three-dimensional interconnected polymeric networks mainly composed of water. They are designed to provide a great, moist environment while protecting the wound from infections.

Many times, additional materials are added to the hydrogel in order to enhance the wound healing process. Foams are porous structures that can absorb high amounts of exudate; thus, preventing wound infections. They can also be used to incorporate ingredients that facilitate and accelerate the healing cycle. [70] Bioactive dressings are made of, or contain, bioactive materials that are useful in wound healing application. They are designed to treat and enhance the natural restorative response of the healing process stages. [71]

The study of nanofiber-based membranes for wound dressings and scaffolds has increased in recent years due to its properties such as high surface area, nano porosity, and the ability to incorporate biomolecules or medications within them. [72] Xu et al. developed a ternary composite nanofiber membrane that could be used in wound dressing applications. The aforementioned membrane exhibited antibacterial activity, cell proliferation, and stability in aqueous medium; these properties are ideal to initiate and enhance the wound healing process. In addition, the fibers were made without the use of toxic solvents, producing a biocompatible and biodegradable product. [73] Akia et al. incorporated South Texas citrus aurantium (bitter orange) juice to nanofibers to produce scaffolds for wound healing that showed an antibacterial activity against Staphylococcus aureus and Escherichia coli of 152% and 71%, respectively, while demonstrating cell adhesion and growth. [74] Sarhan et al. produced honey/chitosan nanofiber membranes for wound dressing applications. A histological examination during the preliminary, in vivo study showed that the fibers enhanced the wound healing process by accelerating the wound closure rate in mice. In addition, the sample exhibited complete bacterial inhibition of Staphylococcus aureus. [75] There are many other studies that examine the properties of biocompatible, biodegradable, and natural products as wound dressings. Currently,

there is no availability of products that can treat all wound types, but with nanofiber membranes, tailor-made solutions can be produced for specific needs.

2.5 Background on Aerogels

Historically, aerogels have been known as synthetic, solid, porous materials produced by replacing the gel's liquid component with a gas. [76-78] With the introduction of new processes to fabricate them, a definition focused on the final material properties has been implemented as follows: a nanostructured network with open pores, high specific surface area, and porosity of at least 90%. [79, 80] The aerogel's three-dimensional structure exhibits extraordinary properties such as extreme low density [81-84], super low thermal conductivity [85-88], high surface area[89], and high porosity [90, 91] among other properties. The impressive properties obtained in aerogels have made them an important field of research, which have resulted in significant contributions and improvements in many applications such as wound healing, scaffolds, filtration, energy storage, sensing application and many more. [92-96]

In 1931, professor Samuel Kistler created the first aerogel by replacing the liquid in a jelly with a gas, which resulted in little to no shrinkage of the structure. He achieved this by exchanging the liquid in the jelly with another, which had a lower critical temperature and didn't disrupt the original structure. Then the jelly was placed inside an autoclave where the vapor pressure and temperature were raised above the liquid's critical pressure and critical temperature. This process converted the liquid to a gas, which was then allowed to escape, subsequently producing an aerogel. [76] Using this method, Dr. Kistler produced alumina, silica, tungstic oxide, ferric oxide, stannic oxide, nickel tartrate, cellulose, nitrocellulose, gelatin, agar, egg albumin, and rubber aerogels. [97] Despite having established this innovative technique, aerogels didn't see any real progress until 1968 when Professor Stanislaus Teichner developed a new

method to fabricate aerogels via sol-gel process. [98] Teichner's approach eliminated the tedious and laborious solvent exchange process which helped reduce the aerogel synthesis time from weeks to days.

2.6 Aerogel Fabrication Process

The general method to fabricate aerogels shown in Figure 2 starts with the formation of a colloidal suspension (sol) derived from precursor particles (i.e. metal alkoxides for inorganic aerogels and organic monomers for organic aerogels). [99] Gradually, particles start branching and cross-linking as development of the gel begins. The addition of a basic or acidic catalyst promotes hydrolysis and condensation reactions to further increase polymerization within the gel and form an interconnected chain structure. Syneresis or aging of the gel is carried out for a period of time, hours to days, according to its process. The gel is maintained in its original solution, where condensation and precipitation reactions within the gel network will continue; thus, increasing the gel's mechanical strength. The last stage is the drying of the gel, where the solvent is removed from the interconnected pore network while preserving its structure. This procedure can be modified with additional processes to produce tailored mechanical, physical, and chemical properties. [100, 101]

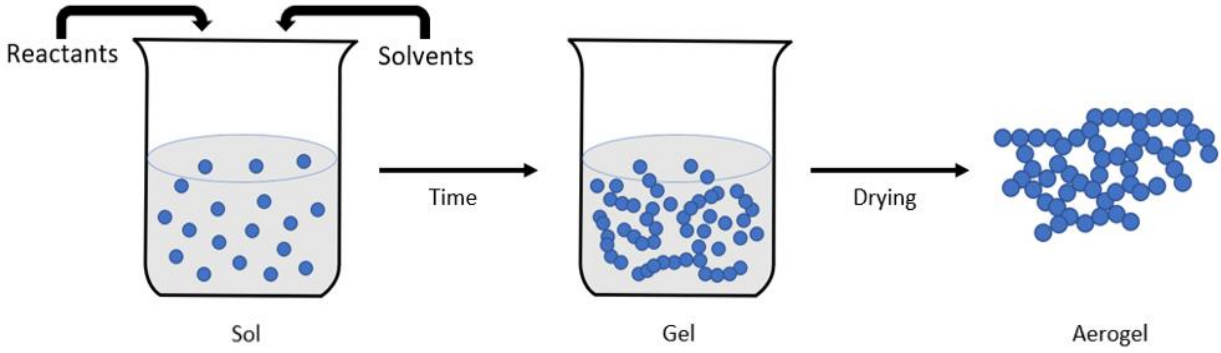

Figure 2. Schematic presentation of the aerogel's synthesis using sol-gel processing.

2.7 Drying Methods of Gels

The drying procedure is a critical step since it determines the final properties of the gel. Since the beginning of the first synthesized aerogel, different drying techniques have been utilized. The most common method is called supercritical drying, but other drying processes, such as ambient drying and freeze drying, have been implemented as well.

The drying mechanism is dictated by capillary pressure. The gel's shrinkage during drying is governed by the capillary pressure, PC, expressed by (1) [102]

$$P_C = \frac{-\gamma_{lv}}{(2(V_p/S_p) - \delta)} \qquad (1)$$

where Υ_{lv} is the surface tension of the pore liquid, V_p is the pore volume, S_p is the surface area and δ is the thickness of the surface adsorbed layer. High capillary stresses can form during the drying process, leading to shrinkage and cracking. To avoid this, a controlled fluid removal process where the liquid surface energy is decreased is necessary.

2.7.1 Supercritical Drying (SCD)

In SCD the pore liquid is removed above the liquid's critical pressure and critical temperature, where the liquid-vapor interface coexists; thus, no capillary pressure is present which results in an almost completely intact porous structure.

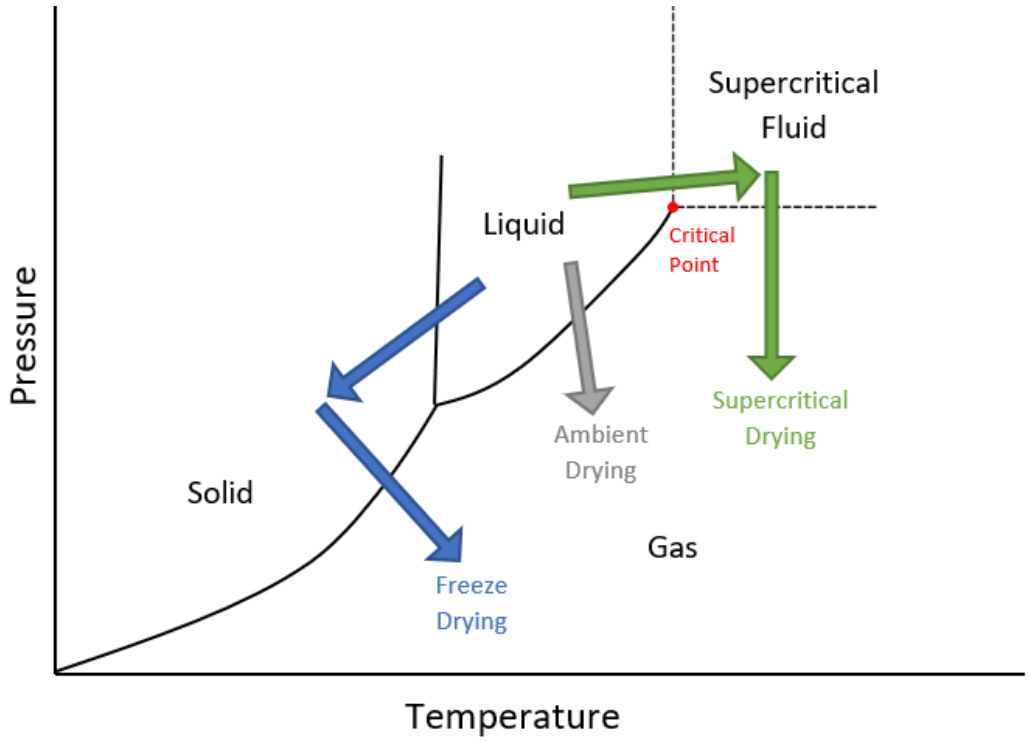

Figure 3. Phase diagram of common processes to dry a gel. The arrows depict supercritical drying, freeze drying, and ambient drying procedures.

The SCD schematic process to achieve the direct conversion of liquid to gas is illustrated in the pressure-temperature phase diagram shown in Figure 3. It consists of placing the wet gel in a closed chamber and gradually raising its temperature to obtain temperatures and pressures that exceed the critical pressure, TC, and critical temperature, TT, of the solvent. Then, while maintaining a constant temperature above TC, the pressure is reduced and the liquid inside the gel is slowly vented. When the exterior pressure is close to the pressure inside the chamber, the sample is cooled to room temperature resulting in a dry, solid sample.

Depending on the temperature needed to obtain a supercritical fluid and the gel's required properties, a hot or cold SCD process is implemented. High-temperature SCD (hot) for organic solvents is an efficient way to minimize shrinkage, producing gels with lower densities than the ones obtained using carbon dioxide (CO2). The materials obtained usually display a hydrophobic

behavior due alkoxy groups found on their surface. However, this method lacks a precise aging process due to the pressure and temperature needed to reach supercritical conditions. [103] In addition, the risk of combustion and explosion at such elevated pressures and temperatures raises safety concerns.

CO2 is used with low-temperature SCD (cold). When using this method of drying, liquid CO2 replaces the gel's organic solvent and is later super critically removed at considerably lower temperatures when compared to high-temperature SCD. A model by Unsulu et al. [104] suggests that using CO2 can result in stresses that don't exceed the strength of the gel-network; thus, no cracking occurs. [105] Also, CO2 greatly reduces the risk of flammability and explosion associated with organic solvents when they reach critical conditions. Unfortunately, due to the exchange of the organic solvent for liquid carbon dioxide, a reorganization of aggregates results in shrinkage of the gel. [102]

2.7.2 Ambient Pressure Drying

An alternative way to dry gels is via ambient pressure drying. During this process the pore fluid is exchange by a low surface tension solvent (e.g. n-hexane or acetone) that facilitates evaporative drying. Furthermore, the gel's surface is chemically modified due to the solvent diffusion which replaces polar surface groups with non-polar groups. Surfactants can be added to reduce surface tension, such that the gel's microstructure is maintained. After the solvent exchange, evaporation at ambient temperature takes place. [101] This method has gained great interest since it provides a cost effective and efficient way to successfully prepare aerogels. [106,107]

2.7.3 Freeze Drying

Freeze-drying, also known as lyophilization, is another method to prepare aerogels. This technique consists of decreasing the gel's temperature below the solvent's crystallization temperature. By controlling the dispersion liquid, freezing rate, and additives the aerogel's macro- and micro- structure can be tailored to specific sizes and alignments. [108] The frozen solvent is then removed by sublimation under vacuum; thus, preventing the formation of a liquid-vapor meniscus and leaving only an interconnected network. Freeze-drying has recently been implemented as a way to fabricate a wide variety of aerogels using nanofiber mats as building blocks, which opens the door for many other aerogel possibilities. Freeze drying can be considered energy intensive, but the chemical waste generated by it is unappreciable. [109]

2.8 Alternative Aerogel Fabrication Process

In 2014, Ding et al. demonstrated a gelation-free, scalable method to develop three-dimensional nanofibrous aerogels by combining electrospun fibers and free-shaping technique; the process consisted of fours steps. First, silicon dioxide (Si02) and Polyacrylonitrile (PAN) nanofibers were produced using electrospinning. The PAN fibers served as the precursor, while the Si02 fibers provided structural stability. Second, both fibers were homogenized in a water/tert-butanol mixture until forming a thorough dispersion of the fibers. Third, the solution was frozen using liquid nitrogen and subsequently placed in a freeze dryer. Fourth, the obtained aerogel was crosslinked via heat treatment to provide elastic resilience. The obtained aerogels exhibited extreme low density, high compressibility, prominent thermal conductivity, effective emulsion separation, high sound absorption, and elasticity-responsive electric conduction. [110]

This solid templating process of nanofibers has been used to create aerogels for a wide variety of applications such as electrical conductivity [111], particle filters [112], energy storage/conversion [113], and oil/water emulsions [114] among many others. The synthesis for such aerogels follows the procedure shown in Figure 4. The method includes three main stages, but additional processes may be incorporated to enhance the aerogel's properties. Preparation begins with the fabrication of nanofiber mats, which are then cut into smaller pieces. Those pieces are then placed in a non-dissolving liquid where they are mechanically homogenized using a dispersion tool, such as a homogenizer, resulting in a dispersion of short nanofibers. The obtained homogenous solution is then transferred to a freezing mold where it gets frozen. As the growing solvent crystals start forming, they start pushing away fibers and entrapping them in between. By controlling the parameters, such as freezing rate, solvent, and fiber loading, properties including pore size and structure can be modified to obtain desired micro and macro structures. Finally, the frozen solution is dried using a freeze dryer, which leaves only the nanofibrous framework known as aerogel. [108] Post treatments can be applied to further improve its properties and achieve tailored applications.

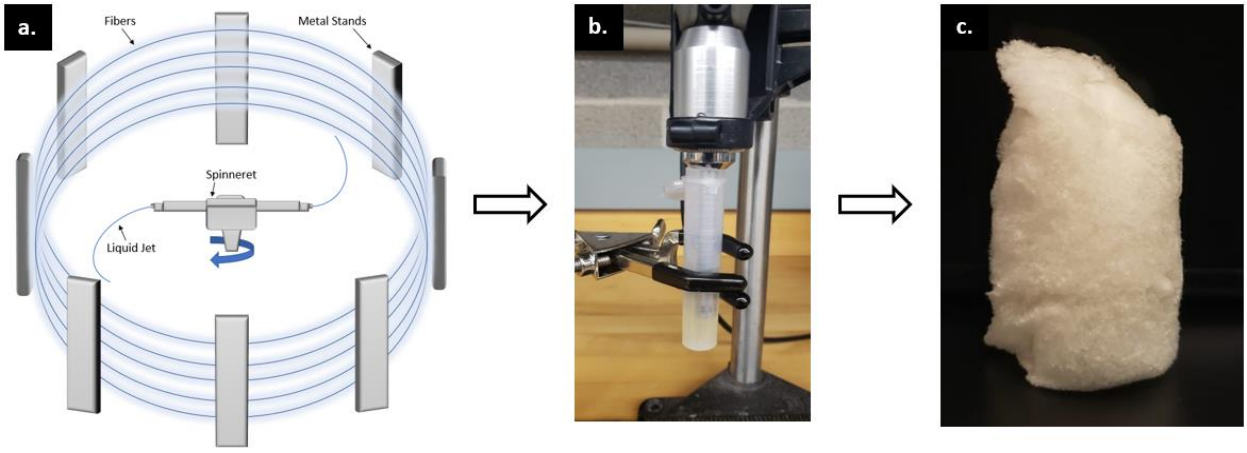

Figure 4. Schematic presentation of the aerogel's synthesis using solid templating. The process starts with the fabrication of nanofiber mats using Forcespinning® Technology (a). The mats are cut into smaller pieces, then homogenized in a non-dissolving liquid (b). The solution is then frozen and dried, resulting in an aerogel (c).

Solid templating allows a facile and scalable process to generate aerogels that exhibit great structural flexibility, stability, and extreme high porosity. [115] The nanofibers' properties remain active in the aerogel, which extends the possibility for the applications of these three-dimensional structures. Only a small portion of the nanofibers have been synthesized into aerogels, but due to the vast and well-established information about them, the opportunities to create novel aerogels using this method are vast and promising.

2.9 Organic Aerogels

Aerogel development has greatly expanded since Kistler's creation of the first aerogel. Currently, there are different categories including inorganic [116-120], organic [121-124], and composite aerogels [125-132], whose properties and applications are based on their building block materials, process, and final structure.

Strong covalent bonds formed from organic precursors allow synthesis of a broad range of organic aerogels. These materials saw a significant growth after Pekala's [121] fabrication of resorcinol-formaldehyde aerogels in 1989. Subsequently, phenol-formaldehyde, melamine-formaldehyde, polyimide, polyacrylamides, polystyrenes, and polyurethanes among other materials were developed. Additionally, carbon aerogels were possible to fabricate as a result of the carbonization of the organic aerogels. [133]

Among the organic aerogels, the polysaccharide-based class has attracted extensive interest due to its properties and applications. These aerogels are synthesized from natural ingredients including cellulose, chitosan, starch, and pullulan, which provide unique features such as biodegradability, biocompatibility, renewability, and low or no toxicity. These properties

offer ideal advantages in the fields of environmental engineering, health, the packaging industry, and buildings among many others. [134]

2.10 Polysaccharide

"Polysaccharides are the macromolecules that belong to the means components of life." [135] They are long chains of polymeric carbohydrate molecules made up of monosaccharide units which are joined together by glycosidic bonds. These biological polymers have highly organized structures that range from linear to highly branched. An important aspect about polysaccharides is their reactive functional groups that can be functionalized to produce a vast range of polysaccharide derivatives. [136] Furthermore, the solubility of polysaccharides is of outmost importance in order to facilitate and expand the number of applications they can be applied to. [137]

Polysaccharides have two main functions: energy storage and structural support. The functions are mainly determined by the carbohydrate structure. For example, linear molecules such as chitin and cellulose are rigid and strong; thus, they serve as the main support molecule in plant, insects, and fungi. The polysaccharides branched structures are usually used for energy storage. These include glycogen and starch, which are found in animals and plants, respectively.

Most polysaccharides can be easily and economically derived from different sources such as microbes, fungi, animals, by products from industrial processes, and plants (which are the most common source of polysaccharides). [138-140] They are primarily obtained by extraction and purification, which serves as a reliable method to improve their yield and quality. [141] Examples of polysaccharides include cellulose, starch, glycogen, chitin, chitosan, and pullulan.

2.11 Pullulan

Pullulan is an extracellular and neutral microbial polysaccharide produced by the fungus Aureobasidium pullulans in sugar and starch cultures. [141] It consists of a linear structure with maltotriose units connected by a (a)-1,6 glycosidic bond. Due to its structure, pullulan is flexible, exhibits a high solubility in water while being insoluble in organic solvents, and is non-hygroscopic. Furthermore, pullulan is biodegradable, nontoxic, noncarcinogenic, nonmutagenic, and edible. It also shows good mechanical strength, decomposes at temperatures of 250-280 C, and can be used to form thin layers, nanoparticles, nanofibers, and flexible coatings. [142]

Pullulan's remarkable properties make it an important source of polymeric materials, which can be utilized in a wide range of applications. Its commercial production began in 1976 in Japan and is currently used in industrial applications such as a blood plasma substitute, food additive, a film, and as an adhesive. [143] The utilization of pullulan for biomedical purposes has attracted a lot of attention due to its inert nature, biocompatibility, low oxygen permeability, and its good chemical and mechanical properties mentioned earlier. Examples include targeted drug and gene delivery [144], medical imaging [145], vaccination [146], and wound healing. [147]

The usage of pullulan for wound healing applications has generated positive results by a number of different investigations. Li et al. [148] synthesized a hydrogel made of a pullulan derivative and cystamine with antimicrobial agents resulting in good swelling capacity, high water absorption, great mechanical strength, effective antimicrobial release activity, and biocompatibility. These results provide outstanding properties as wound dressings for clinical applications. Hydrogels can also be modified to form synthetic dermal scaffolds that serve as structural templates for wound repair. For example, Wong et al [147] fabricated a pullulan-collagen scaffold using a salt-induced phase inversion technique which resulted in an augmented

early wound healing. Pullulan nanofibers membranes also hold great potential for skin tissue engineering. Xu et al. [149] developed a ternary nanofibrous membrane composed of pullulan, chitosan, and tannic acid that showed non-cytotoxicity, antibacterial properties, enhanced cell proliferation and attachment, good water stability and absorption.

2.12 Aloe Vera

Aloe vera (also known as Aloe vera (L.) Burm.f.) is a type of succulent plant that belongs to the Aloaceae family. [150] It has been used medicinally for centuries in numerous cultures for a variety of purposes due to its high biological activity. The aloe leaf is composed of three layers: 1. the outer green rind, which serves as a protective layer as well as synthesizes proteins and carbohydrates [151]; 2. the middle layer of latex, whose main and active components are hydroxyanthrancene derivatives (15-40%) such as the anthraquinone glycosides aloin A and B [152]; and 3. the inner clear gel, which consists of about 99.5% water while the remaining 0.5% is made up of a wide range of compounds.

Aloe vera contains more than 75 potentially active constituents including minerals, vitamins, amino acids, saccharides, enzymes, lignin, anthraquinones, salicylic acids, and saponins. There are a number of studies trying to identify and evaluate which of these substances are responsible for its healing effects. However, some research suggests that the synergetic interaction between the compounds, rather than a single component, is what produces its beneficial properties. [153] For example, numerous reports investigating the benefits of Aloe vera have shown positive results in burn-wound treatments [154, 155]; wound healing [156, 157]; scaffolds [158, 159]; and antibacterial [160], antiviral [161], and immunostimulative activity[162], among other health advantages.

CHAPTER III

EXPERIMENTAL TECHNIQUES

3.1 Forcespinning

Forcespinning® is a process employed to make nanofibers (NFs) using centrifugal force instead of electrostatic force as in electrospinning. This process allows a facile way of producing fibers and an increase in yield. In Forcespinning®, material in the form of polymer solution is deposited in the spinneret and then it is centrifugally forced through specific orifices to form a polymer jet. As the polymer solution jet starts evaporating, it produces a continuous fiber that gets deposited in between designed collectors placed around the spinneret. The controllable parameters that influence the fiber include spinneret's angular velocity, viscoelasticity of solution, surface tension, solvent evaporation rate, distance from collector, temperature and humidity.

Once the desired amount of fibers are formed, different collection mechanism can be employed. For example, the fibers can be collected in a uniaxial method where all the fibers are aligned in one direction or multiaxial process to have fibers aligned in 2 or more directions. Rotating cylinder can be utilized to collect fibers, this process collects fibers in a constant directional approach while improving fiber elongation. A schematic is shown in Figure 5.

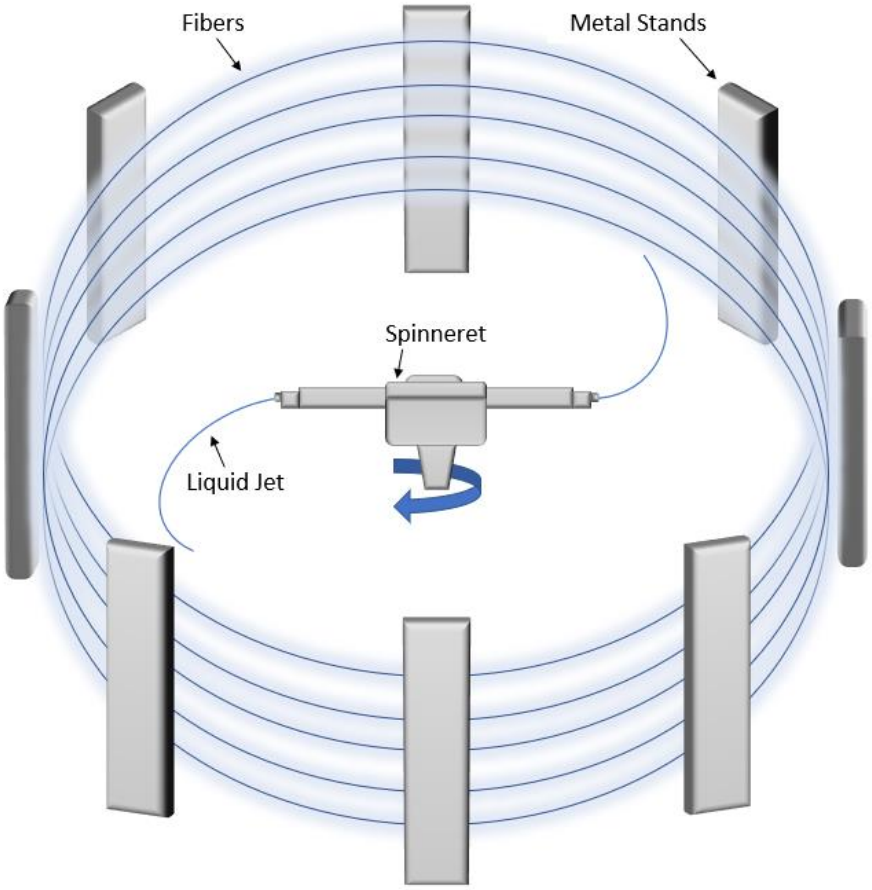

Figure 5. Centrifugal force mechanism

3.2 Fourier Transform Infrared

A Fourier Transform Infrared (FTIR) Spectrometer is used to identify chemical bonds in a molecule, which are then used to characterize and analyze different materials including solids, liquids, and gasses. The instrument collects broadband near infrared and far infrared spectra by obtaining a sample signal's interferogram and then applying a Fourier Transformation on it, yielding a spectrum.

In an FTIR spectrometer, an IR-beam enters the interferometer and is directed at a beam splitter which splits the beam into two separate beams. One beam is transmitted through the beam splitter to a fixed mirror while the other one is reflected and directed at a moving mirror.

The light travels back to the beam splitter where is recombined and is then directed at the sample's material. This allows the spectral information of all wavelengths to be acquired simultaneously. The detector produces raw data representing the intensity of light as a function of the position of a mirror. This signal is then Fourier-transformed to produce the IR plot of intensity vs. wavenumber. The spectrum data produced by the FTIR is like a chemical fingerprint which enables the characterization of new materials or identify and verify unknown and known samples.

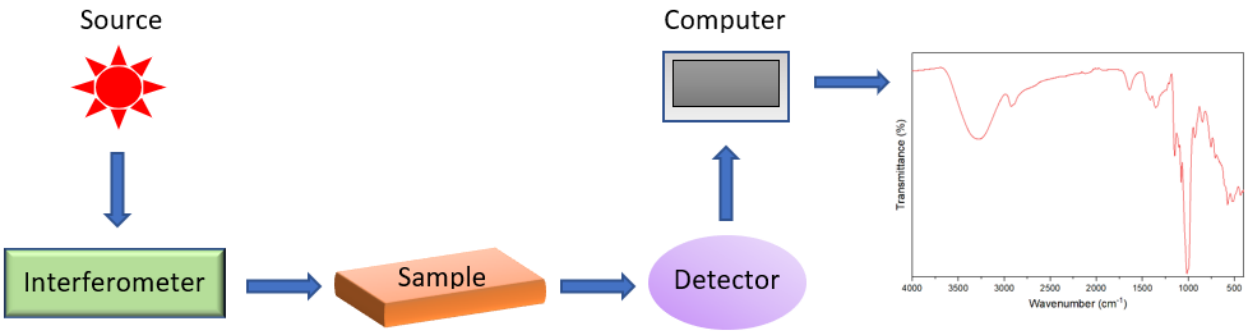

Figure 6. Schematic diagram of a FTIR spectrometer.

3.3 Scanning Electron Microscope

The Scanning Electron Microscope (SEM) provides information about the topography and composition of a sample. SEM main components include an electron source (also called electron gun), electron lenses, sample chamber, electron optical column, detectors, display or data output devices. The function of the SEM is based on the electron behavior after electron-sample interaction. An electron beam which carries electrons with a significant amount of kinetic energy interacts with the sample. Some of these accelerated electrons pass through the sample and some scatter elastically and inelastically. The elastic or inelastic scattering of electron results in different signals including secondary electrons, backscattered electrons, characteristics X-rays, auger electrons, visible lights, and heat. Some of these signals provide imaging, quantitative and

semiquantitative information of the sample. Secondary electrons are mostly advantageous for morphological and topological information while backscattered electrons are advantageous for distribution information of various elements in the sample. The signals are detected with electron detectors and processed for a detailed image of the sample surface.

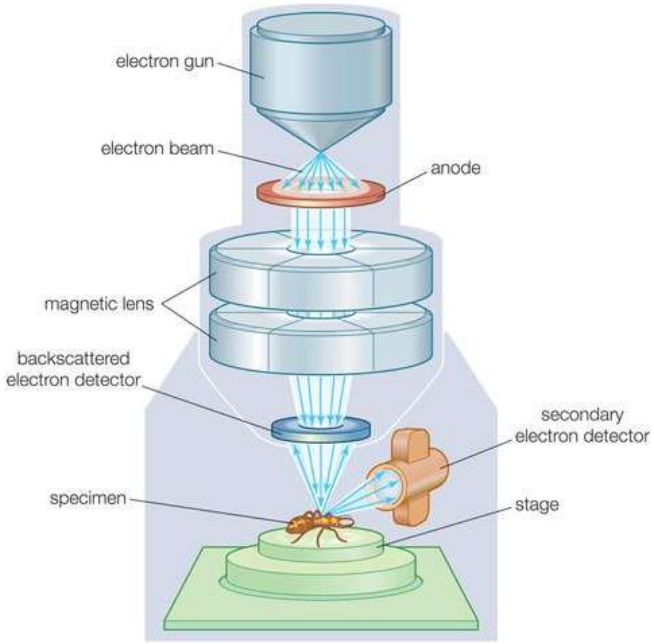

Figure 7. Schematic diagram of a SEM. [163]

3.4 Homogenization

Homogenizer is an equipment used to homogenize different materials such as liquids, powders, fibers, plants, and many others. Generally, this tool is employed to mix two or more different materials that are non-soluble. The homogenizer breaks the liquid or solid into small particles that are then distributed among the solution. Since the particles are greatly reduced in size, they tend to stay mixed in the solution without separating; hence, making the solution homogeneous.

The homogenizer has a rotor-stator component, which rotates at speed up to 30,000 RPM. The high-speed rotations cause the liquid and/or solid to move into the rotor and then outward using centrifugal forces. By doing this, the solid or liquid collides at high speeds with the blades outside the rotor reducing the particles size. The liquid or solid goes through this process several times, reducing the size of the particles each time, until the desired mixture is attained.

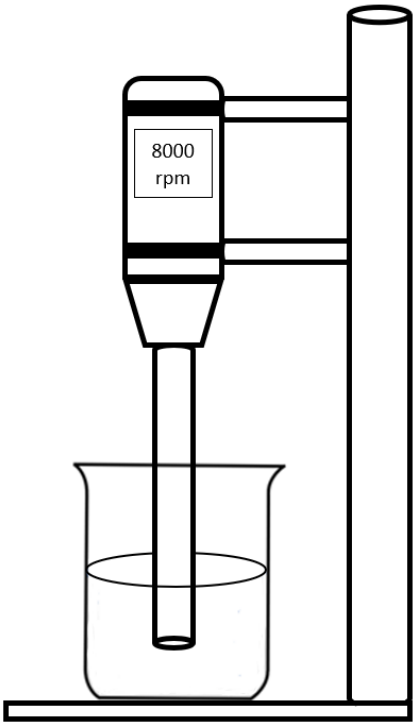

Figure 8. Schematic of a homogenizer.

3.5 Biological Studies

3.5.1 Antibacterial Analysis

To test and examine the antibacterial properties of the fibers, the disk diffusion method was performed. All composite fiber samples were tested against Gram negative Escherichia coli (E. coli), a bacterium typically found in wounds. Each sample was cut using a coring tool with a 1 cm diameter to obtain disk-shaped specimens. Then, 25 mL of sterilized agar was poured into

individual sterilized plates, followed by the introduction of the bacteria. The bacteria were then spread evenly throughout, and the cut specimens were placed in them using two replicates per sample. Subsequently, the plates were placed in an incubator at 37˚C for 24 hours.

3.5.2 Cell Culture

NIH 3T3 mouse embryonic fibroblast cells were chosen to study cell adhesion and behavior. The cells were cultured in Dulbecco's Modified Eagle's Medium (DMEM), supplemented with 10% fetal bovine serum (FBS), 100IUmL−1 of penicillin, and 100μgmL−1 of streptomycin. Cells were maintained at 37°C in a humidified incubator with 5% CO2.

3.5.3 In Vitro Cell Process

For in vitro cell adhesion and viability studies, the composite NF membranes were cut at approximately 7 x 7 mm and placed in a 6-well cell culture plate. The samples were then sterilized under ultraviolet (UV) light for 10 minutes. In order to evaluate cell proliferation, 120,000 NIH 3T3 cells were seeded per sample in a 3-trail experiment, and incubated for 2, 4, and 6 days. After incubation, samples were first treated with Mito Tracker Red (MTR) for 20 minutes followed by phosphate buffer saline (1XPBS) washes to remove non-adherent cells. Next, they were fixed with 4% formaldehyde for 30 minutes and stained with 300 nm 4′,6-diamino-2-phenylindole (DAPI) for 5 minutes. Afterward, membranes were washed twice with 1xPBS and mounted with 50% glycerol. Cells were prepared and viewed using an Olympus FV10i confocal laser scanning microscope.

3.6 Thermogravimetric Analysis

Thermogravimetric analysis (TGA) is a thermoanalytical technique where the sample's mass is measured over time as a function of temperature under a controlled atmosphere. There are two main methods for TGA testing, one is static or isothermal thermogravimetry where a sample is heated at a constant temperature for a determined amount of time. The second method is the dynamic thermogravimetry which increases the temperature at a constant rate until the set temperature is acquired. The results from these measurements are presented in a plot of mass as a function of temperature or time. The data depicts weight loss of the material due to oxidation, sublimation, vaporization, decomposition, sublimation, and absorption. This information represents the amount of organic and inorganic compounds in the sample, decomposition peaks temperature, residues and degradation temperatures. As a result, a decomposition profile, life expectancy, percentage of solvent, filler, and plasticizer can be quantified.

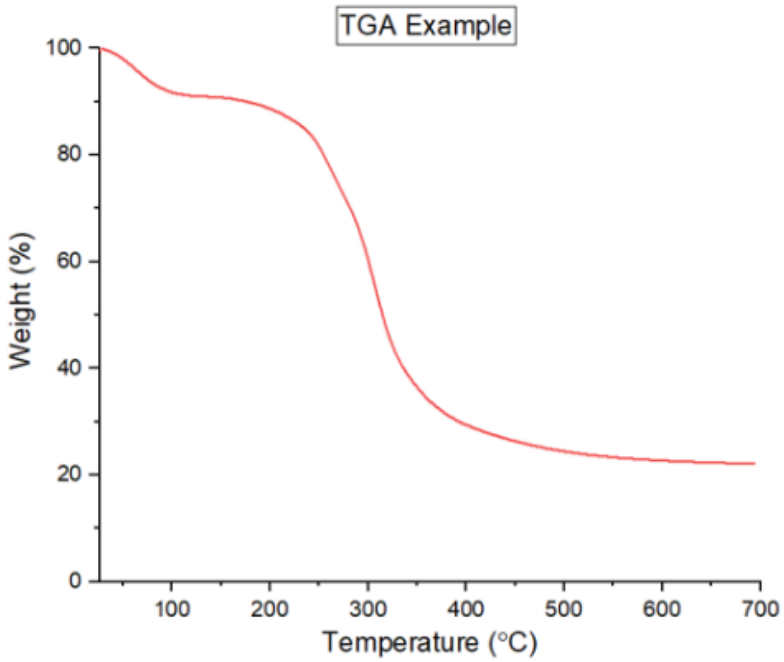

Figure 9. TGA example graph showing a sample's degradation path.

CHAPTER IV

METHODOLOGY

The fibers were produced using four steps shown in figure 10 which consisted of: 1. preparing the solution, 2. production of fibers, 3. collection of fibers, and 4. thermal cross link of the fibers. The obtained fibers were analyzed to determine thermal-physical, antibacterial, and cell growth proliferation properties.

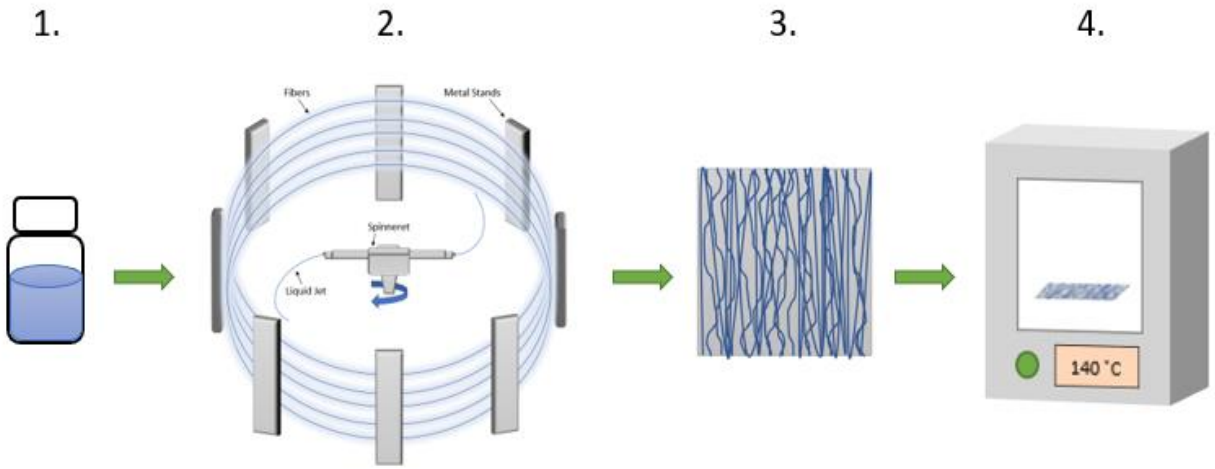

Figure 10. Schematic procedure of the method used to prepare, make, and cross-link NFs.

4.1 Materials and Methods

4.1.1 Materials

Pullulan (PL) was purchased from Tokyo Chemical Industy Co. (Japan). Chitosan (CH) with a low–molecular weight (MW = 50,000–190,000 and 75%–85% degree of deacetylation)

was purchased from Sigma–Aldrich (St Louis, USA). Citric Acid (CA) was purchased from Sigma–Aldrich (St Louis, USA). Aloe vera leaf was filtered and used without further treatment. Deionized (DI) water was produced from a Smart2Pure water purification system. 30-gauge (half-inch) bevel needles (PrecisionGlideTM) were purchased from Fisher scientific for the use of fiber production process.

4.1.2 Aloe Vera Extract Preparation

An Aloe vera leaf was washed with DI water and dried at ambient temperature. The leaf was cut from both ends and left to drain excess liquid. The bottom flat side of the leaf was skinned and was once again rinsed with DI water to ensure a clean specimen. A sanitized spatula was used to scrape off the Aloe vera extract (AVE) which was then placed in a glass container. The collected extract was filtered using a 50 μm syringe filter. The filtered AVE was collected into a separate glass container and stored in a fridge at 15˚C for further experimental use

4.1.3 Solution Preparation

For the control solution (control), 10 mL of DI water was placed in a 20 mL vial and mixed with 400 mg of CA until completely dissolved. Then, 500 mg of CH were added to the aqueous solution and vortexed until homogeneity was achieved. The CA/CH solution was left to stir over night using a magnetic stirring rod. Later, 2 grams of PL were added to the CA/CH solution, homogenized, and left to stir for a minimum of 6 hours.

For the remaining solutions, different AVE/DI water concentrations were prepared in order to observe the influence of the AVE concentration on the fiber diameter, thermal stability, antibacterial effect, and cell growth proliferation. The AVE/DI water ratios (v/v) consisted of

2/8, 6/4, and 10/0 mL per solution and were designated as 20%, 60%, and 100% extract, respectively. The CA, CH, and PL were added following the same steps as the control procedure.

4.1.4 Forcespinning Process

Forcespinning® process uses centrifugal forces to create NFs in a controlled chamber with adjustable parameters such as angular velocity and time. These helps to ensure a good quality and quantity of fiber production with respects to external conditions. To produce the fibers, a 3 mL syringe was used to inject 2 mL of the prepared solution in a spinneret of a Cyclone™ L-1000M, purchased from FibeRio Technology Corporation (McAllen, USA). The prepared solution was spun at an RPM ranging from 4000 to 7000 which permitted the solution to successfully exit through the spinneret's orifices. The solution was ejected from both ends of the spinneret through the 30-gauge needles, and was elongated onto equally distanced vertical pillars, thus creating composite NFs which were then collected with a 10x10 cm collector after each cycle. NFs were laid on top of one another in a uniform manner after each collection per cycle to ensure a composite NF membrane. They were later covered and stored in a low moisture environment.

4.1.5 Cross-linking

Once the Forcespinning® process was complete, the collected NF membranes were placed in an oven at 140˚C for 1 hour to allow proper chemical cross-linking with CA. The cross-linking process allows the composite NFs to be insoluble in water and increase its thermo-physical properties. The sample was then taken out of the oven and left to dry for further analyzation.

4.1.6 Aerogel Preparation

The cross-linked composite NF membrane with a weight of 80 mg was cut into pieces of 1 x 1 cm^2 and dispersed in 8 mL of DI water. The solution was then mechanically homogenized using a PRO Scientific Bio-Gen PRO200 homogenizer for 5 minutes at 12,000 rpm resulting in a dispersion of short NFs. The obtained homogenous solution was then transferred to a mold and frozen at -82˚C. The frozen solution was subsequently dried using a Freezone 4.5 freeze dryer system for 24 hours, leaving only the nanofibrous framework known as aerogel. This process was repeated for the 20%, 60%, and 100% extract NFs. The generated aerogels were labeled AG-control, AG-20%, AG-60%, and AG-100% (derived from the samples they were made of).

4.2 Characterization

4.2.1 SEM Analysis

A SEM (Σigma VP-ZESS) was used to analyze the morphology and average diameter of the composite NFs obtained (Fig. 11). The magnifications range from 300X to 1500X and a voltage of 1-3kV was used throughout the process. The NFs average diameter was calculated by indiscriminately measuring the diameter of 100 different fibers from SEM images using the image analysis software ImageJ.

Figure 11. Σigma VP-ZESS Scanning Electron Microscope

4.2.2. TGA

TGA was completed using a Netzsch TG 209, shown in Figure 12, at a rate of 10 ˚C/min, with temperatures increasing from room temperature to 700˚C in a nitrogen atmosphere. All the samples analyzed weighed 10 mg each.

Figure 12. Netzsch TG 209 Tarsus

4.2.3 FTIR Analysis

Samples with a 1 x 1 cm were cut and placed inside the Thermo Nicolet NexusTM 470 FT-IRESP FTIR machine (Fig. 13). The background spectrum was removed, then the samples were scanned in range of 400–4000 cm^{-1} with a resolution of 4 cm^{-1}.

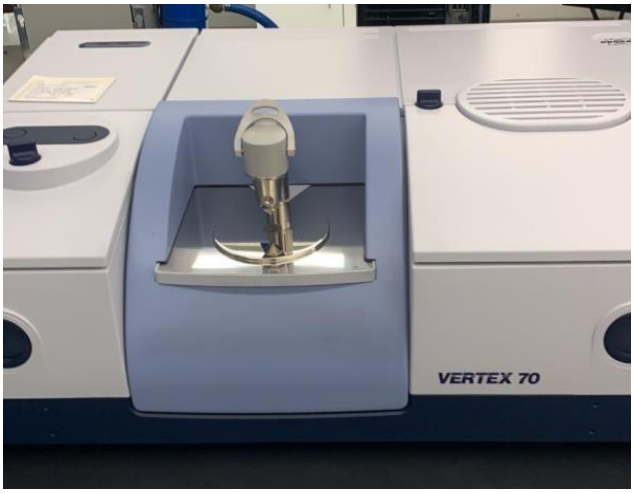

Figure 13. Bruker Vertex 70 FTIR Equipment

CHAPTER V

RESULTS AND DISCUSSIONS

5.1 Morphology of Composite NF Membranes

Forcespinning® (FS) technology was chosen due to its high yield of NFs, combined with the wide variety of materials from which it can produce NFs. An optimization analysis of the composite NFs was performed and found the optimum parameters to be 5500-6500 rpm in a humidity of 45-55%. The photographs, SEM micrographs, and fiber diameter statistical analysis of the developed samples are shown in Figure 14 as a, b, and c respectively. To further enhance structural stability of the composite membranes and avoid their dissolvement in liquids, they were cross-linked at 140˚C for 60 minutes in an air atmosphere. During this process the CA functioned as a non-toxic cross-linking agent, which caused the membranes to change from white to beige (Figure 14(a)). All the NFs obtained from FS exhibited long, smooth, and continuous fiber morphology, illustrated in Figure 14(b). The control sample had the lowest mean fiber diameter of 528 nm and a standard deviation of 146 nm, while the 100% extract specimen showed the highest mean fiber diameter of 906.9 nm and a standard deviation of 320 nm. The data showed a positive correlation between the mean fiber diameter and the increase in AVE (Figure 14(c)). The cross-linked membranes were submerged in water, removed, and analyzed under SEM (Figure 15). These CA cross-linked composite NF membranes show an improved water stability compared to the non-cross-linked samples, which dissolve when they interact with water.

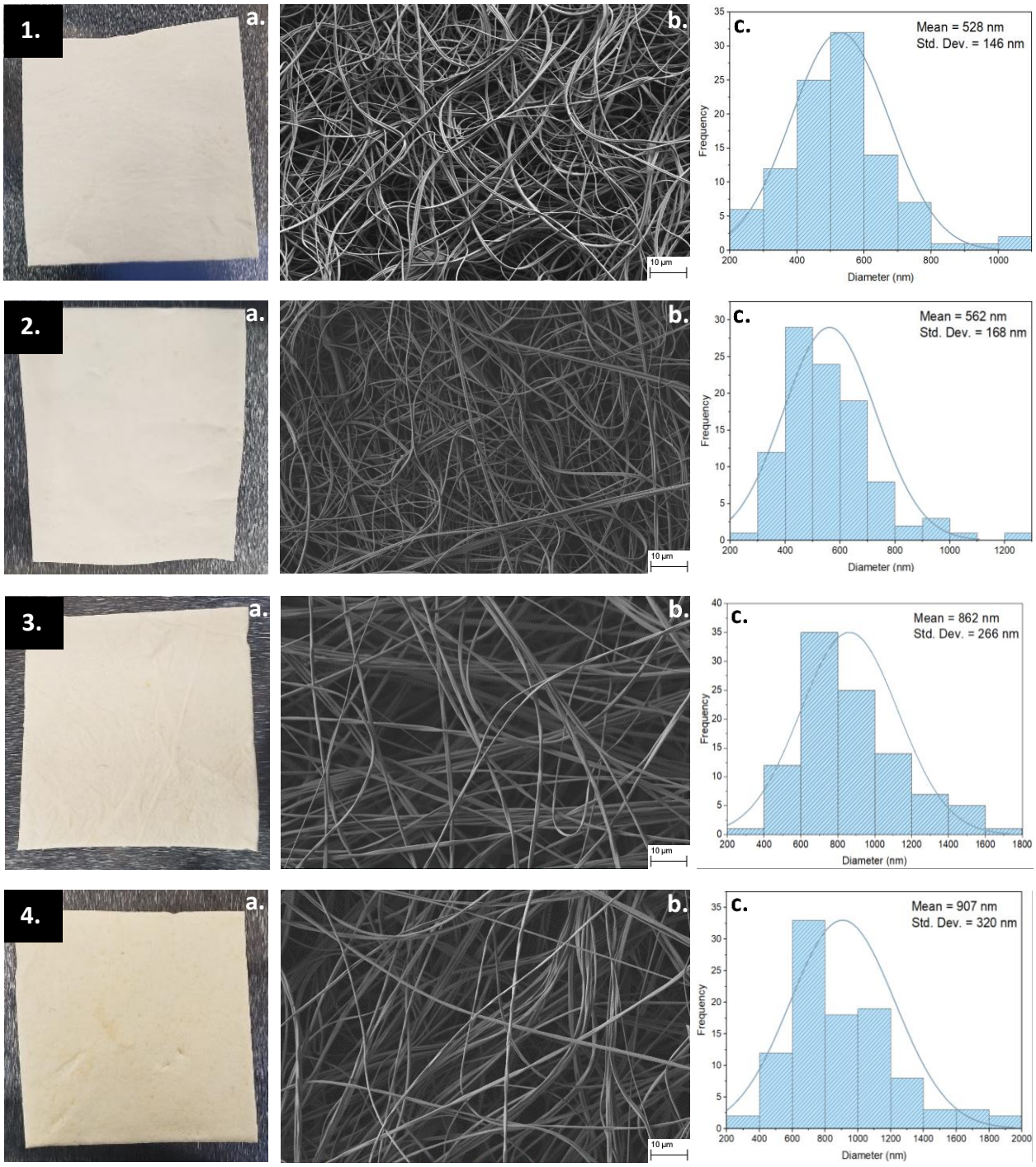

Figure 14. The images labeled as 1, 2, 3, and 4 represent the control, 20% extract, 60% extract, and 100% extract, respectively. Photographs of the cross-linked composite NF membranes (a), scanning electron microscope (SEM) micrographs (b), and fiber diameter distributions (c).

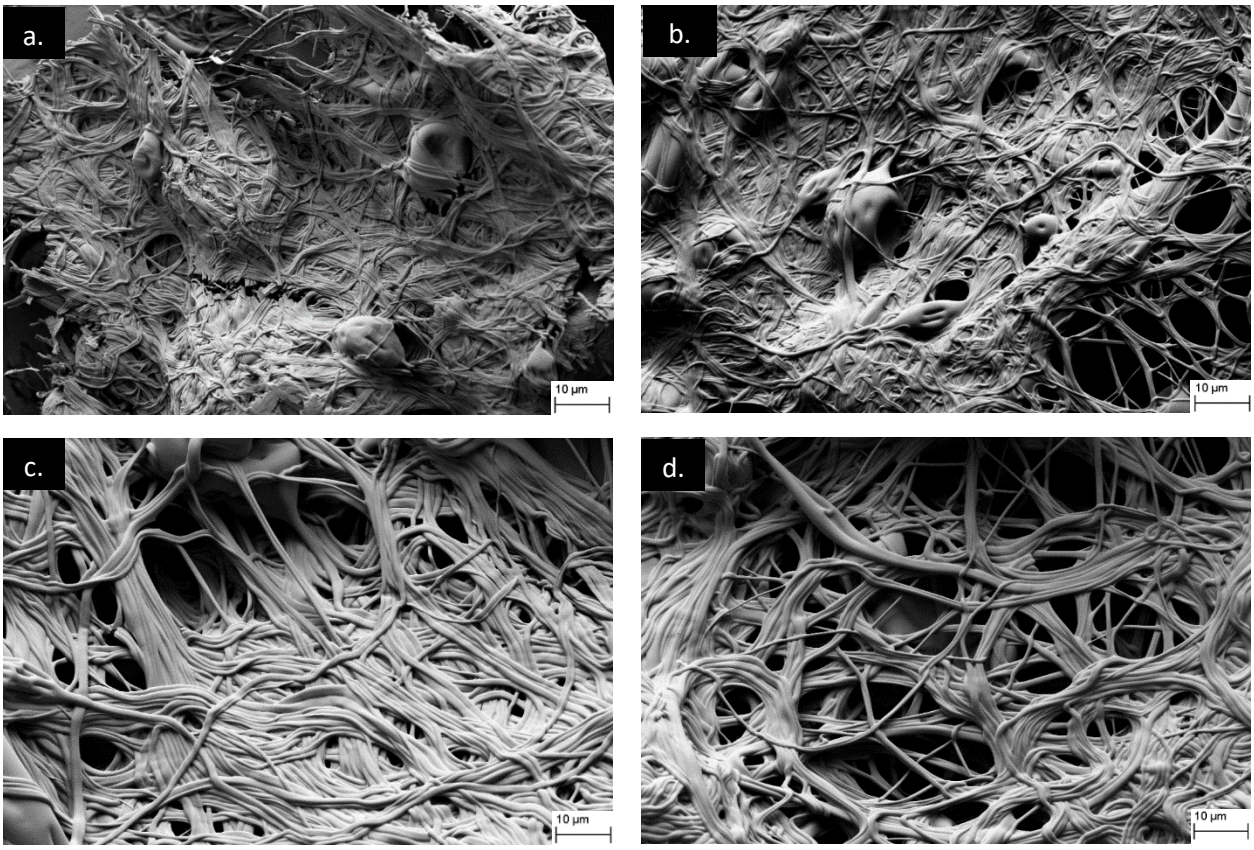

Figure 15. Image of cross-linked NFs, control (a), 20% extract (b), 60% extract (c), and 100% extract (d), after being submerged in water.

5.2 Antibacterial Assessment of Composite NF membranes

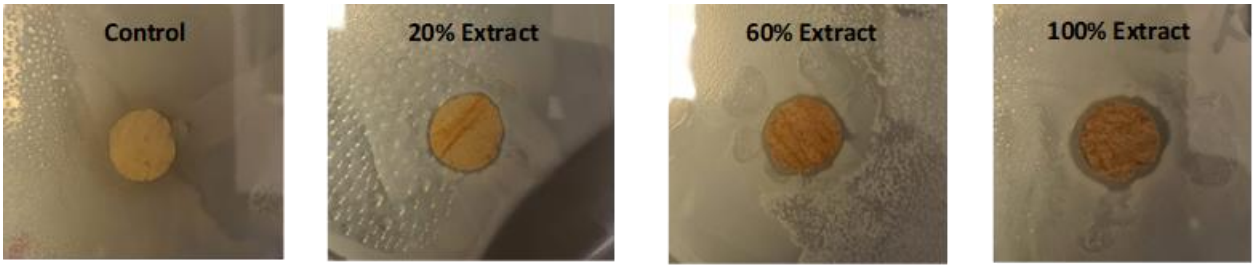

Figure 16. Image of cross-linked composite NF membranes tested against Escherichia coli.

As seen in Figure 16, the cross-linked composite NF membranes exhibit clear rings around the samples, known as inhabitation zones, indicating antibacterial activity. The samples resulted in inhabitation zones of 0.5 mm, 1 mm, 2 mm, and 2.5 mm, respectively. These results

illustrate that the antibacterial properties of the composite NFs membranes were enhanced as the concentration of AVE increased.

Aloe vera is used in skin related treatments due to its antifungal, anti-inflammatory, antiviral, and antibacterial activity against multiple types of infections. Previous studies of Aloe vera's antibacterial properties against gram negative E. Coli and other bacteria have also demonstrated effective antimicrobial efficacy. [164] The mechanism by which Aloe vera exerts its antibacterial action is believed to be associated to anthraquinones. Anthraquinones act as tetracycline, which blocks the ribosomal A site, thus, inhibiting the bacterial protein synthesis and preventing the bacteria from growing. [165] Furthermore, Aloe vera possess a hydroxylated phenol known as pyrocatechol, which is proven to be toxic to micro-organisms. The number of present hydroxyl groups on the phenol group is correlated to the level of micro-organism toxicity (i.e. the more hydroxyl groups present, the more toxic to micro-organisms). These phenolic groups are responsible for the cell membrane disruption, as well as the denaturing of bacterial cell protein. Additionally, other studies have reported the ascorbic acid found in Aloe vera, acts as a strong antibacterial agent that inhibits enzymatic activity and interferes with bacterial cell membrane and genetic mechanisms. [166] The amount of active biological components present in the samples are essential for the antibacterial activity as observed in the results obtained.

5.3 In Vitro Cell Adhesion and Proliferation in Composite NF membranes

MitoTracker Red CMXRos is a cell-permeable red fluorescent dye that accumulates in the negatively charged mitochondrial matrix and allows for detection of the mitochondrial membrane potential. The mitochondrial membrane potential is a key indicator of cell health or injury; healthy cells accumulate more dye compared to apoptotic cells. [167] DAPI staining is a

technique used to determine a cells viability by identifying its nuclear morphology in colocalization assays. [168]

Cell adhesion and proliferation were analyzed on the composite NF membranes after 2, 4, and 6 days (shown in Figure 17). It was observed that the MitoTracker stains were present in all samples, which indicated that the cells were active within the nanofibrous membranes, with the exception of day 4 of incubation in the 60% extract sample. Additionally, a constant detection of the red dye remained throughout the following days, which demonstrated that the cells maintained their initial health. Furthermore, cell nuclei are clearly apparent in all samples, with a constant number of cells appearing each day. There was a significantly high number of cells on day 6 for the 60% extract sample and the presence of clusters within some of the other NF composites. A cell spread is exhibited with an increase of AVE, as compared to a rounder cell morphology present in control samples.

Using 10 images per sample an average cell count was calculated and an Anova post-hoc Tukey statistical analysis was conducted (Figure 18). A significant difference was shown in the 60% extract sample when compared to the control at day 4. At day 6, all samples were shown to have no significant difference to the control. This could be based on the variation between the values found in each respective sample, as shown through the high standard error bars. The results suggest that the composite membranes were not found to be toxic to the cells, and cells can effectively attach and proliferate onto these biocompatible nanofibrous membranes.

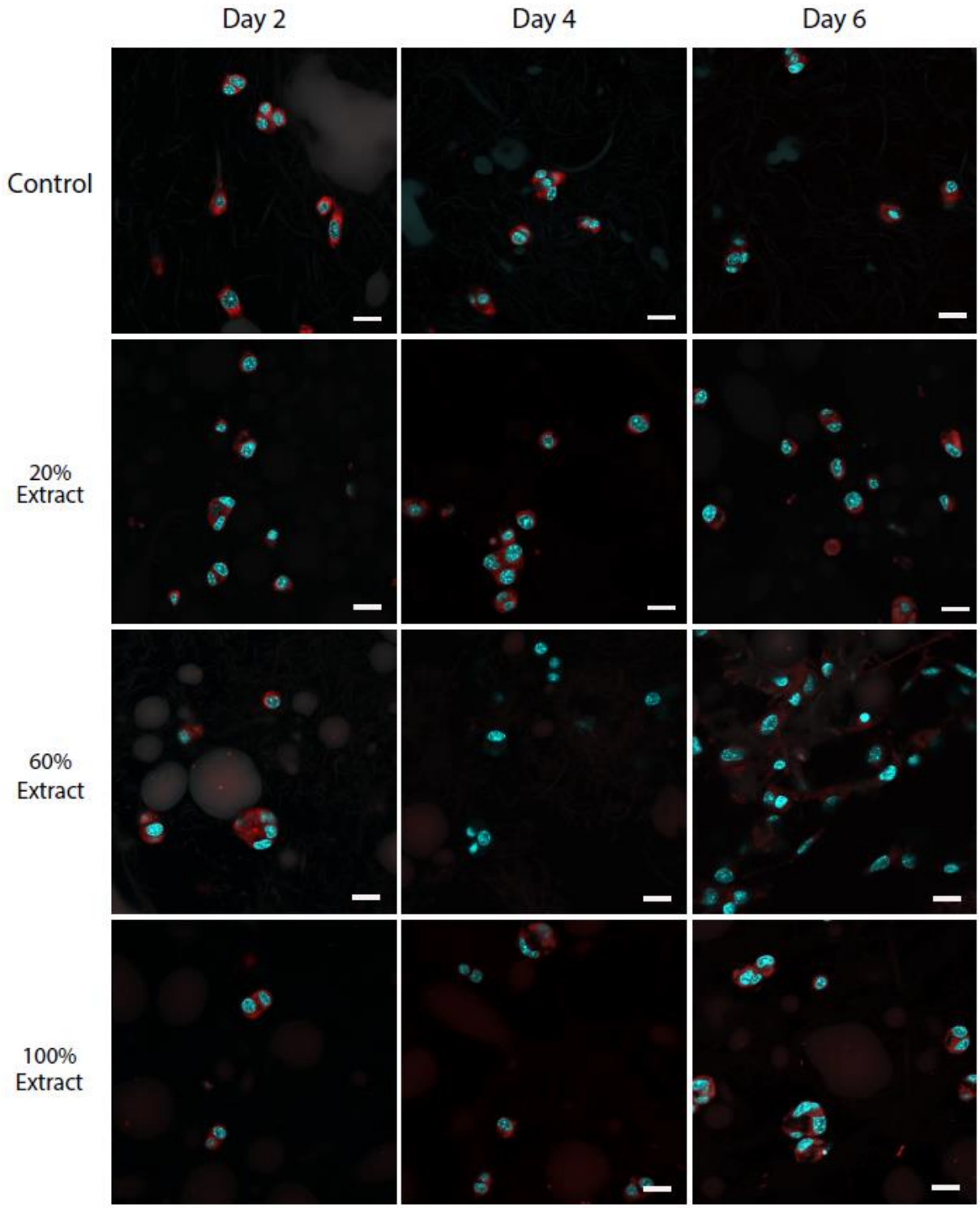

Figure 17. Confocal microscopy of NIH 3T3 cell adhesion and proliferation in cross-linked composite NF membranes.

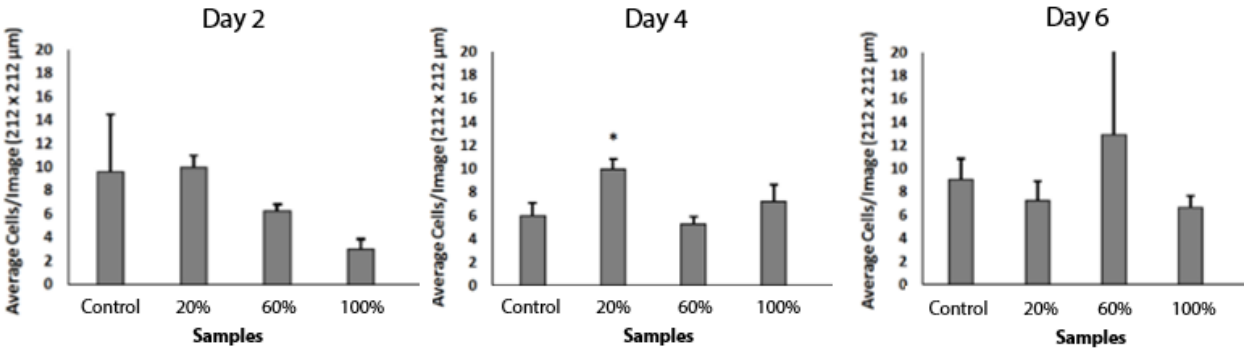

Figure 18. Cell proliferation results from a 3-trial experiment for cross-linked composite NF membrane samples: control, 20%, 60%, and 100% extract.

5.4 TGA Evaluation of Composite NF membranes

Different thermogravimetric measurements were performed to analyze the thermal stability and the effect of Aloe vera extract in the cross-linked composite NFs. The TGA and DTGA thermograms of the samples are shown in Figures 19 and 20. The lyophilized Aloe vera extract followed multiple degradation steps, starting with the loss of water content observed between 26˚C to 135˚C. Then the degradation process began and a weight loss at 210˚C to 290˚C, attributed to hemicellulose decomposition, was recorded. Decomposition of cellulose and lignin were observed between 300˚C and 395˚C and in the range from 400˚C to 520˚C, respectively. After 520˚C the weight loss was minimal due to the presence of fixed carbon. [169, 170]

All the AVE composite NFs show a weight loss over two stages. The first one occurred between 26˚C and 150˚C, caused by the loss of structural water in the samples. The second stage was the thermal degradation of the polymers starting at 150˚C. During this stage decomposition of the material began by the partial breaking of the molecular structure and disintegration of intermolecular bonds. [171] As the AVE content increased, the NFs exhibited a lower decomposition onset temperature (To), attributed to the initial thermal degradation of the AVE.

Solaberrieta et al. obtained similar results; a decrease of the onset temperature decomposition with increasing AVE content in the polyethylene oxide (PEO) NF formulations. [172] Furthermore, the addition of AVE resulted in a small decrease in the maximum rate of thermal degradation temperature (T_{max}). Even though the addition of AVE caused small changes in the T_o and the T_{max}, it didn't affect the overall decomposition of the samples. A residual mass of 18.37%, 19.06%, 19.62%, and 20.12% for the control, 20%, 60%, and 100% extract, respectively, reflected the higher amount of AVE in their system.

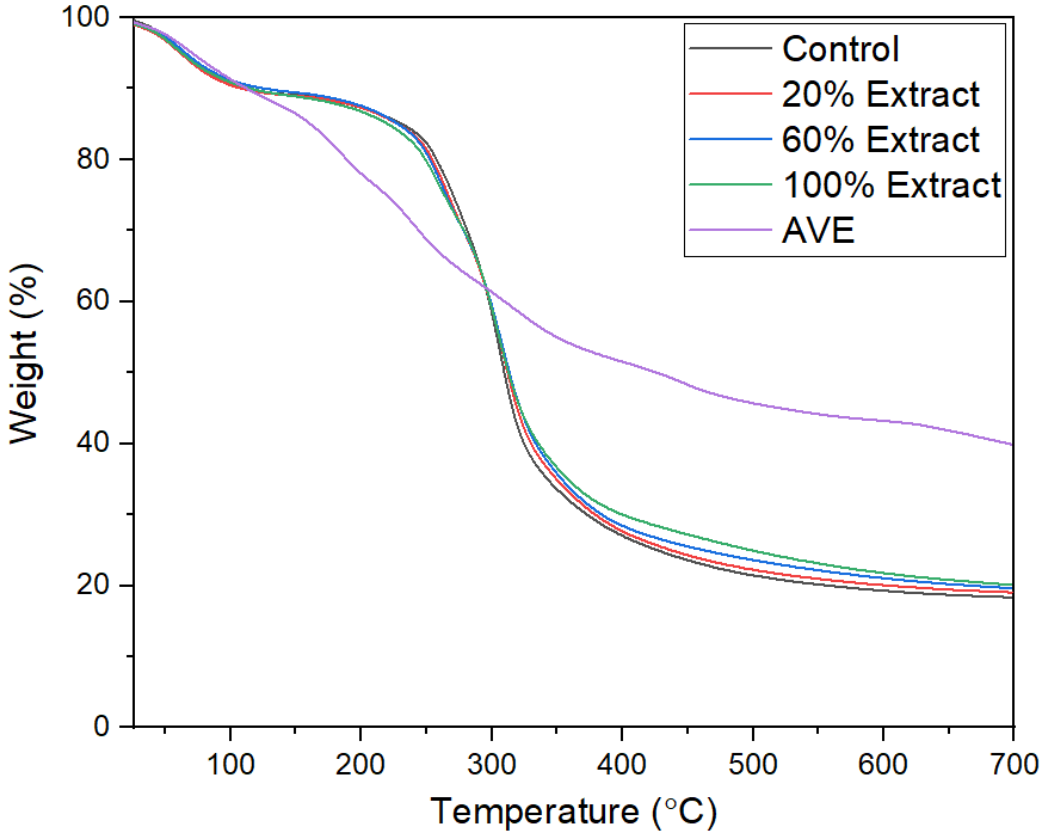

Figure 19. TG analysis of the cross-linked composite NFs and lyophilized Aloe vera extract.

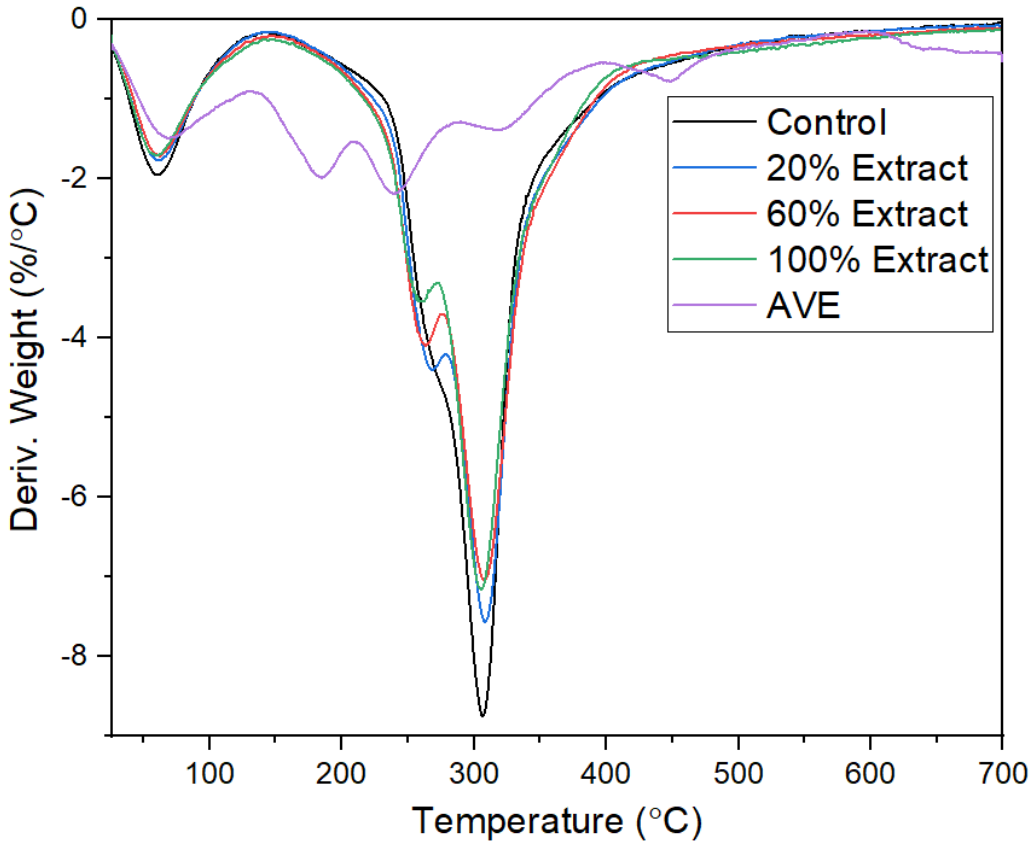

Figure 20. DTG analysis of the cross-linked composite NFs and lyophilized Aloe vera extract.

5.5 FTIR Analysis of Composite NF membranes

The FTIR analysis was used to assess the functional groups present in the individual components, as well as the composite NFs. In Figure 21 we can observe the infrared spectrum of chitosan powder, pullulan NFs, and the composite NFs. For pullulan, the broad band in the region around 3278 cm^{-1} was attributed to the O-H stretching and hydrogen bond originating from water molecules. The band at 2923 cm^{-1} corresponded to the C–H stretching. [173] A single band at 1,639 cm^{-1} was attributed to the stretching vibration of O–C–O. Other features were also observed in the spectra including C-O (1018 cm^{-1}), C–O–C stretch (1,148 cm^{-1}), and C–O–H bend (1,356 cm^{-1}), as reported by Singh and Saini. [174] An intense characteristic band of pullulan was located at 1078 cm^{-1}, which was due to the large proportion of the primary C-

OH groups at the C-6 position. This band was absent in the spectra for the chitosan, but it remained at 1078 cm^{-1} on the composite NF membrane, indicating that the added components did not affect the vibrational behavior for the C–OH group. [175,176]

In the chitosan spectra, a broad band at 3288 cm^{-1} corresponds to the O-H and N-H stretching. [177] The absorption bands at around 2870 cm^{-1} is ascribed to the asymmetric C-H stretching, which are typical characteristics of polysaccharides. The bands at 1645 cm^{-1} (C=O stretching of amide I) and 1319 cm^{-1} (C-N stretching of amide III) confirmed the presence of residual N-acetyl groups. Characteristic absorption bands at 1584 cm^{-1}, 1419 cm^{-1} and 1374 cm^{-1} corresponded to the NH2 bending of the primary amine, CH2 bending, and the distorting vibration of C-CH3, respectively. [178, 179] Additionally, the band at 1149 cm^{-1} can be attributed to C–O–C stretching vibration in the glucopyranose ring, and the absorption band of at 895 cm^{-1} corresponds to the β(1 → 4) glycoside bridge structure. [180]

The composite NFs shows a new band at 1714 cm^{-1}, which is attributed to the C=O stretching vibration due to the carbonyl group in CA. The absorption band at 847 cm^{-1} is attributed to the α-configuration of α-D-glucopyranose units which decreased from the pullulan NFs as a result of the addition of CS, which contains β-glycosidic bonds. [181] Furthermore, bands found in the pullulan NFs spectra appeared in the composite NFs, including the bands at 754 cm^{-1} and 928 cm^{-1}, which prove the presence of pullulan's two main linkages: α-(1,4) glucosidic bonds and α-(1,6) glucosidic bands, respectively. [182]

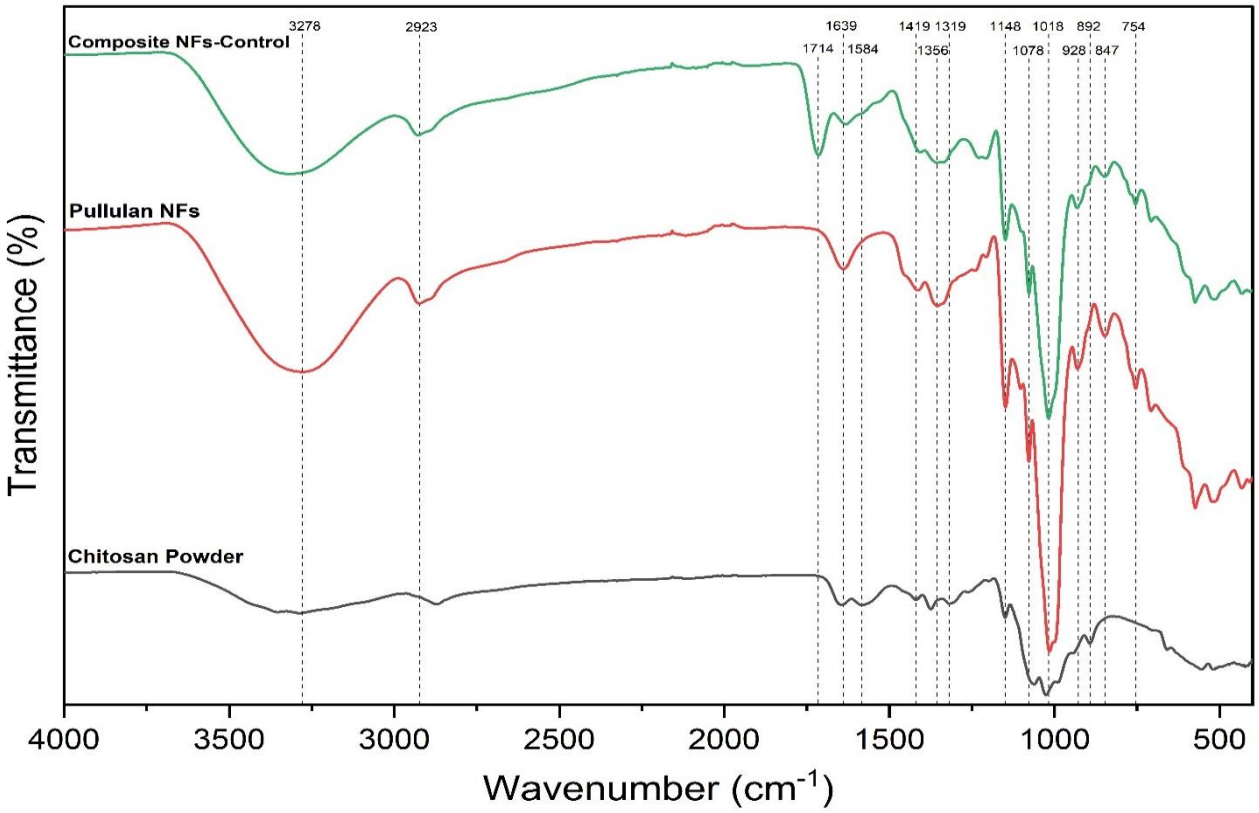

Figure 21. FTIR spectrum of the composite NF control sample (a), pullulan NFs (b), and chitosan powder (c).

The Aloe vera spectrum shown in figure 22 illustrates a peak at 2927 cm^{-1} associated to the symmetrical and asymmetrical C–H stretching of the −CH2 groups, indicating the presence of aliphatic (−CH) groups in these compounds. Absorption at 1714 cm^{-1} indicates a carbonyl peak (C=O) belonging to acids, ketones, and aldehydes. [183] The absorption bands at 1580 cm^{-1} and 1393 cm^{-1} are attributed to the C═C stretching and the symmetrical –COO stretching of carboxylate compounds in Aloe vera, respectively. Stretching vibrations of C–O groups of esters and phenols are attributed to the absorption at 1244 cm^{-1}. [184, 185] Furthermore, the shoulder peak at 1077 cm^{-1} has been related to the C−O stretching associated with rhamnogalacturonan, and the high intense band at 1017 cm^{-1} corresponds to the C−O and C−OH bonds of the glucan units in polysaccharides. [186]

It was noted that an increase in the AVE content used to prepare the composite NFs reflected a subtly higher absorption band at 1580 cm^{-1}. Different authors have shown that the peak around 1600 cm-1 demonstrates the inclusion of Aloe vera and natural extracts such as grape seed and rosemary in NFs. [172] After cross-linking, the band at 1207 cm^{-1} was slightly enhanced as a result of the etherification reaction between the hydroxyl and carbonyl groups of pullulan and CA. [187] The combination of pullulan, CA, CS, and Aloe vera did not have any substantial changes in the chemical composition, which allowed them to maintain their individual properties. As a result, the thermal stability, antibacterial, and biological effects were maintained.

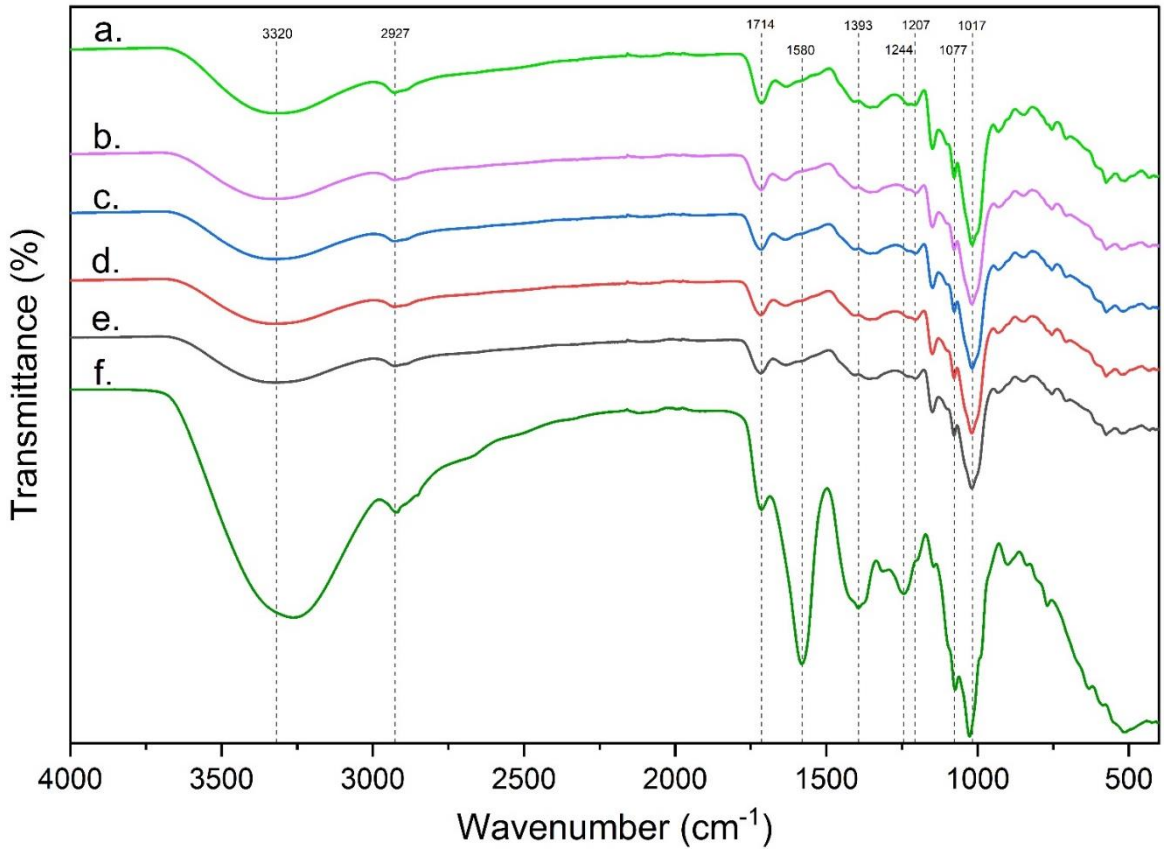

Figure 22. FTIR spectrum of the composite NF control sample (a), cross-linked composite NF control sample (b), cross linked composite NFs with 20% extract (c), cross-linked composite NFs with 60% extract (d), cross-linked composite NFs with 100% extract (e), and lyophilized Aloe vera extract (f).

5.6 Morphology of Aerogels

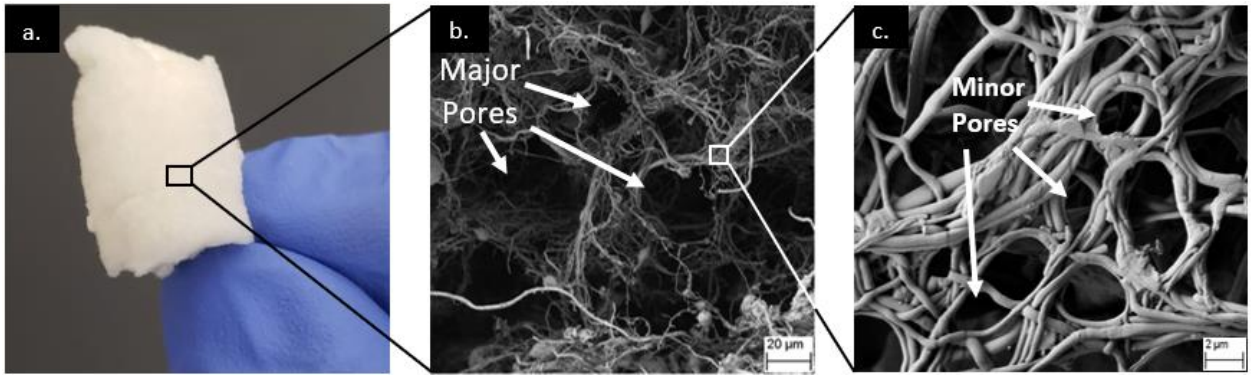

Figure 23. Photograph of aerogel (a) with SEM images illustrating its major (b) and minor (c) pores.

The aerogel's structure (Figure 23(a)) was derived from the process of freezing the solution which contained the NFs and the non-dissolving liquid; the growing solvent crystals caused the NFs to be pushed away and become embedded. The removal of the solvent crystals by sublimation yields a nanofibrous framework characterized by major (Figure 23(b)) and minor (Figure 23(c)) pores. The porosity and pore size can be modified through different mechanisms such as fiber loading, freezing rate, and solvent. For example, increasing the fiber loading will result in an aerogel with lower porosity due to a higher volume of NFs inside the solution, while the freezing rate and solvent can be manipulated to obtain specific major pore sizes.

Figure 24 shows the morphology obtained from AG-control, AG-20%, AG-60%, and AG-100%. The major pores formed by the solvent crystals range in diameter from 20-80 μm in all samples. This size range can be attributed to the fact that water was used for all the samples, thereby obtaining a similar crystal growth rate and size. The minor pores, with sizes of 2-6 μm, are located between the tangled NFs; the ones found in the aerogels are in the same size range as those in the NFs. It was observed that the AG-control had the largest minor pore sizes, while the AG-100% had the smallest. A thicker fiber diameter found in the AG-100% reduced the space

between the fibers, consequently producing reduced minor pore sizes. The interconnection between major and minor pores produced an open-pore network which can serve a wide range of applications. [188]

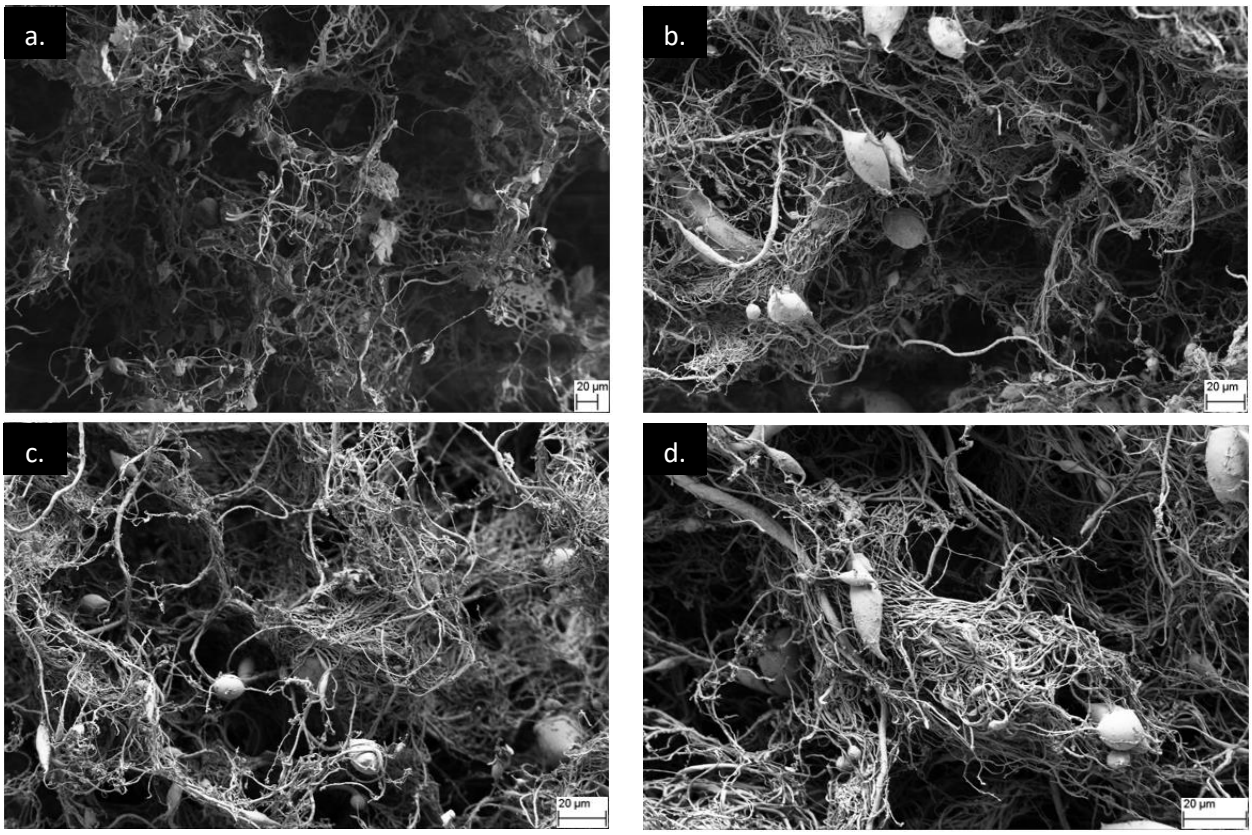

Figure 24. The images labeled as a, b, c and d represent the AG-control, AG-20%, AG-60%, and AG-100%, respectively.

5.7 Antibacterial Assessment of Aerogels

Figure 25 illustrates the clear rings around the aerogels, known as inhabitation zones, indicating antibacterial activity. The samples AG-control, AG-20%, AG-60%, and AG-100% resulted in an inhabitation zones of 0, 0.5, 2, 3 mm, respectively. These results illustrate that the antibacterial properties of the composite NF-based aerogels were further enhanced as the concentration of AVE increased.

The mechanism by which Aloe vera exerts its antibacterial action is attributed to anthraquinones, pyrocatechol, ascorbic acid, and cinnamic acid. These compounds prevent bacteria from growing via bacterial protein synthesis inhibition, cell membrane disruption, and interference with the membrane and genetic mechanisms. The amount of active biological components present in the samples are essential for the antibacterial activity as observed in the results obtained.

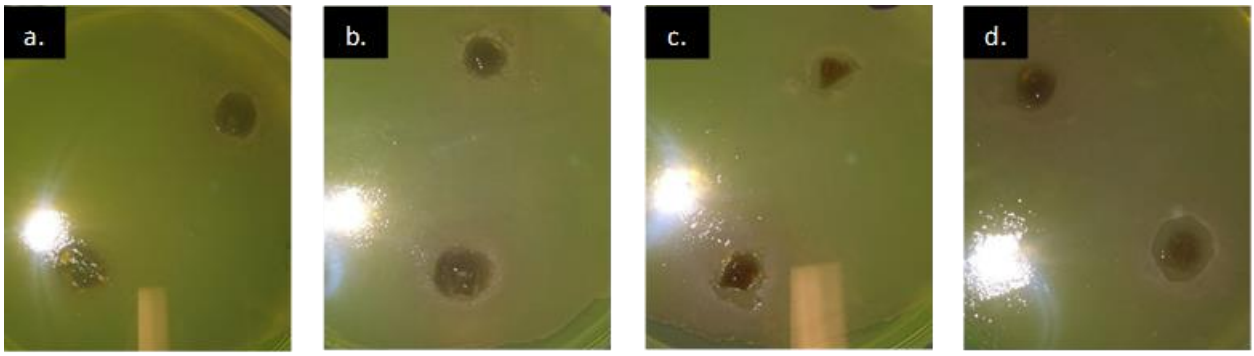

Figure 25. Image of composite NF-based aerogels tested against Escherichia coli. Starting from the left with AG-control (a), AG-20% (b), AG-60% (c), and AG-100% (d).

5.8 In Vitro Cell Adhesion and Proliferation in Aerogels

MitoTracker Red fluorescent dye allows for detection of the mitochondrial membrane potential. The mitochondrial membrane potential is a key indicator of cell health or injury; healthy cells accumulate more dye compared to apoptotic cells. [167] DAPI staining was used to determine the cells' viability by identifying its nuclear morphology in colocalization assays. [168] Cell adhesion and proliferation were analyzed on the composite NF-based aerogels for 2, 4, and 6 days (shown in Figure 26). It was observed that the MitoTracker stains were present in all samples, which indicated that the cells were active within the aerogel. In addition, a constant detection of the red dye remained throughout the following days, which demonstrated that the cells maintained its initial health. Furthermore, cell nuclei were clearly apparent in all samples

with a constant number of cells appearing each day. Another clear observation is the cells' morphology; they remained constant with a round cell morphology similar to that of previous NF control samples, which may be attributed to suspended cells. After 6 days cells remained with a constant presence among all samples.

Figure 27 displays the average cell count per sample (10 images were captured/trial/sample for each individual day) where a One-way ANOVA Post-hoc Tukey statistical analysis was conducted. Based on the data, AG-20% and AG-60% had a slightly higher cell presence than the AG-control. The aerogel samples differ from NFs in which cells are shown to exhibit a closer interaction within a NF-based form, as compared to the visible round morphology exhibited within an aerogel. The results suggest that the NF-based composite aerogels are not toxic to the cells, allowing them to effectively proliferate and attach onto these biocompatible aerogels.

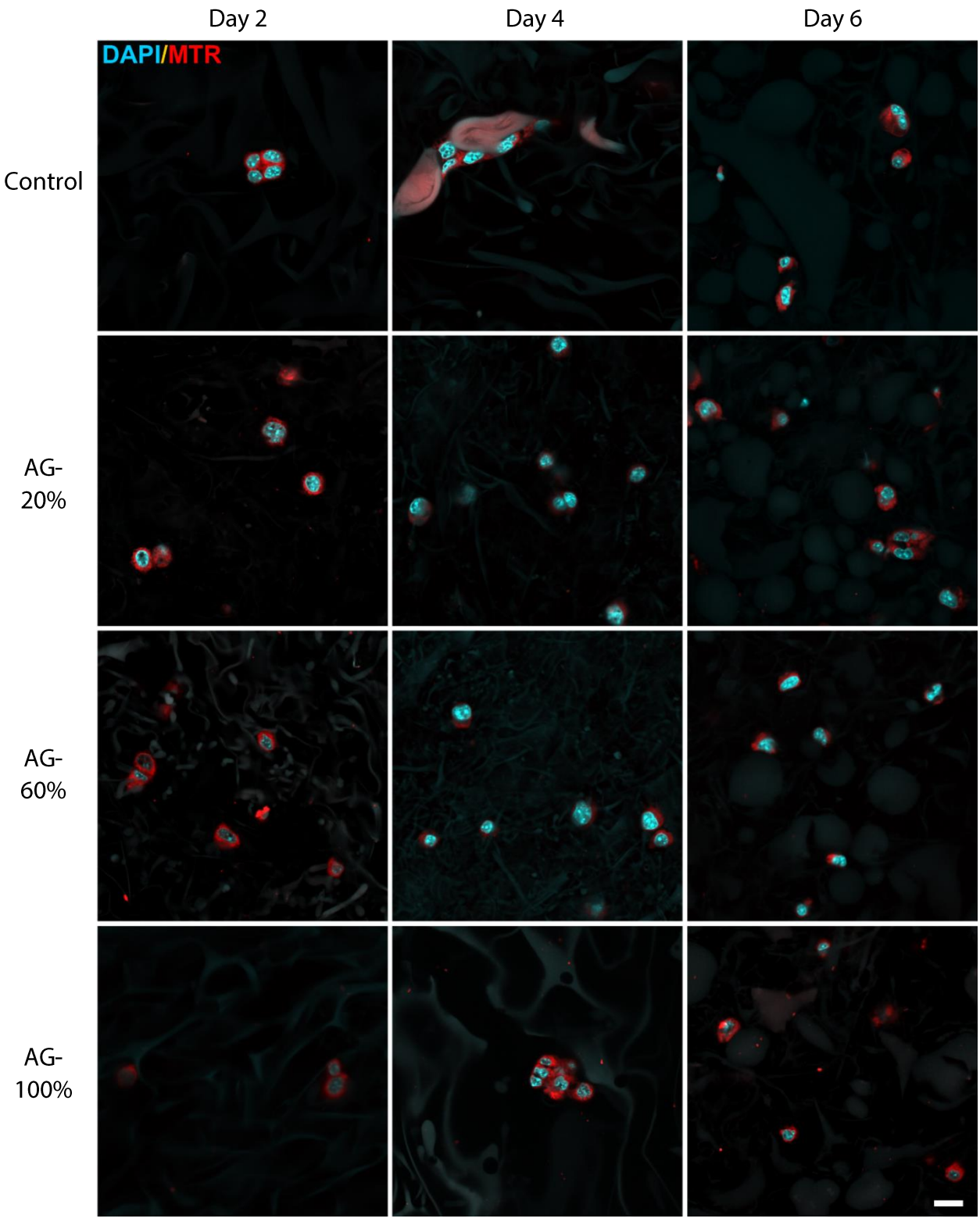

Figure 26. Confocal microscopy of NIH 3T3 cell adhesion and proliferation in composite NF-based aerogels.

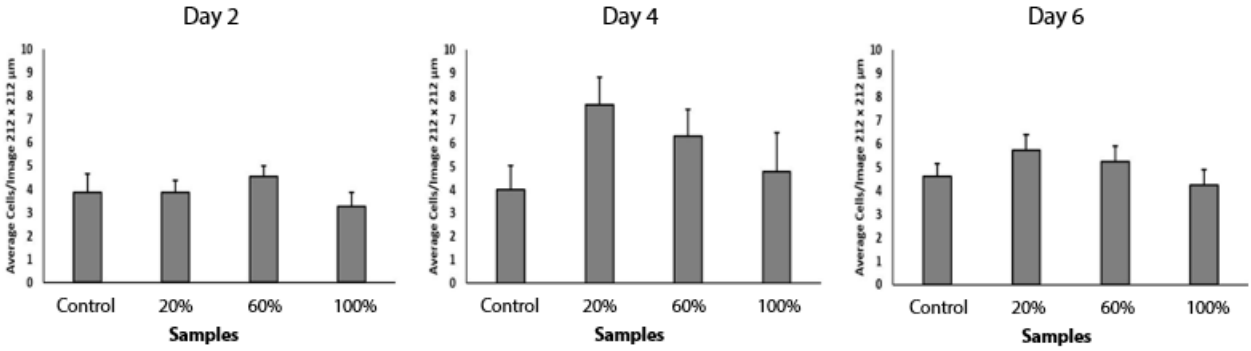

Figure 27. Cell proliferation results from a 3-trial experiment for fiber-based composite aerogels samples: AG-control, AG-20%, AG-60%, and AG-100% extract.

5.9 TGA Evaluation of Aerogels

The TGA and DTGA thermograms of the composite NF-based aerogels are shown in Figures 28. All samples show a two-step weight loss behavior very similar to the cross-linked composite NF membrane. The first step was the loss of structural water in the samples between 26˚C and 150˚C, followed by the thermal degradation of the polymers starting at 150 ˚C. During this stage decomposition of the material begins by partial breaking of the molecular structure and disintegration of intermolecular bonds. [171] The aerogel samples with AVE exhibited a higher decomposition onset temperature (T_o) compared to the AG-control. AG-20% exhibited the greatest change follow by AG-60% and AG-100%, with an increase in the T_o of 5%, 4%, and 2%, respectively. The addition of AVE caused a small increase in the T_o which was opposite to the results obtained from the composite NF membranes. Nonetheless, those minor changes didn't affect the overall decomposition of the samples. Moreover, a residual mass 18.10%, 19.66%, 20.25%, and 20.99% for the AG-control, AG-20%, AG-60%, and AG-100%, respectively, reflected the higher amount of AVE in their system.

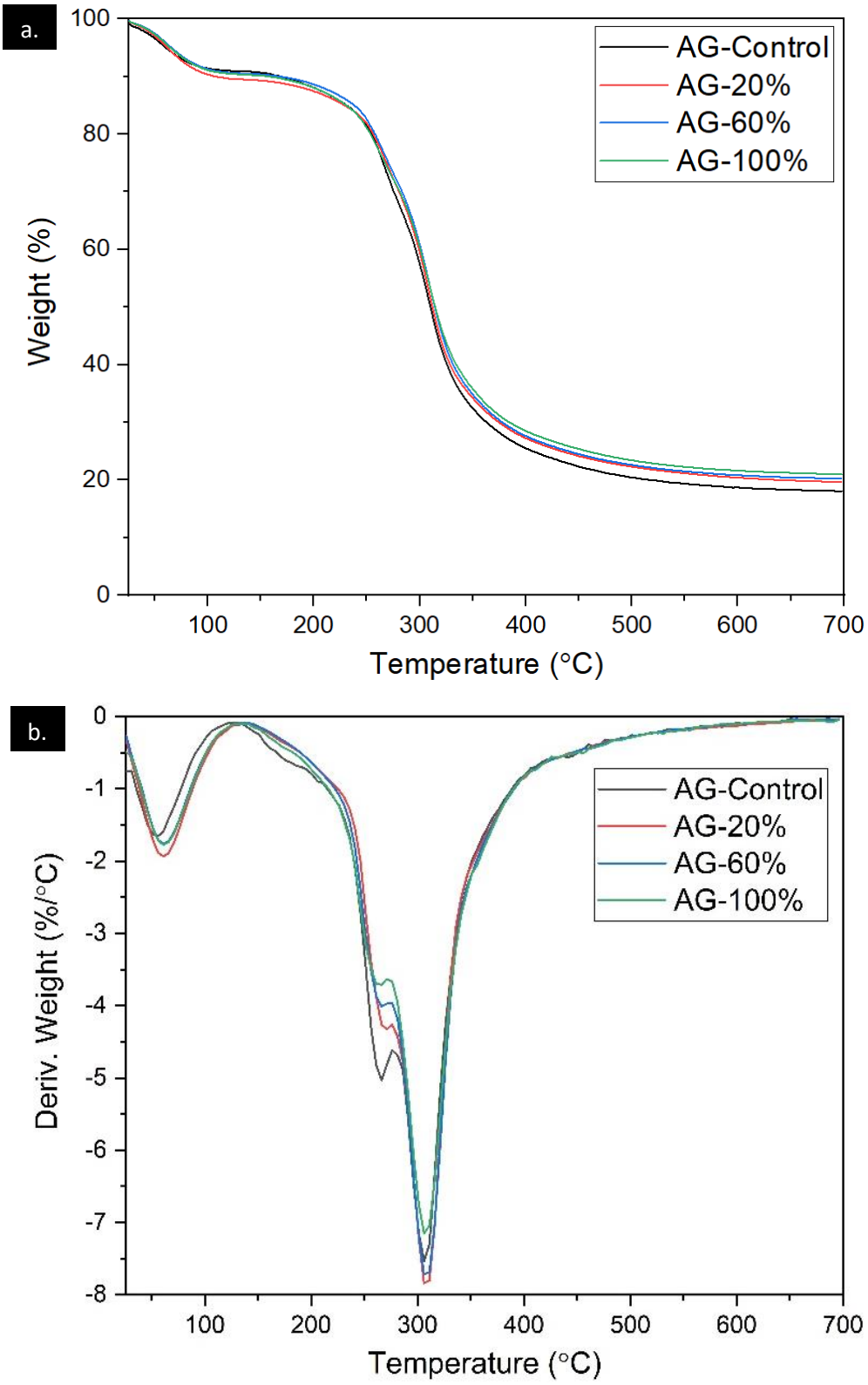

Figure 28. TGA (a) and DTGA (b) of the fiber-based composite aerogels.

5.10 FTIR Analysis of Aerogels

The AG-Control shows the same characteristic peaks as the composite NF control sample, indicating that they have the same composition. Both show the band at 1714 cm^{-1}, which is attributed to the C=O stretching vibration due to the carbonyl group in CA. In the aerogel samples, an increase in Aloe vera content used to prepare the composite NFs membranes reflected a slightly higher absorption band at 1580 cm^{-1}. This trend confirmed the successful incorporation of Aloe vera in the membranes as reported by Solaberrieta et al. [172] Furthermore, the band at 1206 cm^{-1} was slightly enhanced as a result of the etherification reaction between the hydroxyl and carbonyl groups of pullulan and CA, respectively. [187] Also, the characteristic shoulder peak at 1077 cm^{-1} related to C−O stretching associated with rhamnogalacturonan, and the high intense band at 1017 cm^{-1} associated with the C−O and C−OH bonds of the glucan units in polysaccharides were noted. [186] No differences were found between the composite NFs and the composite aerogels, which confirms that both share same characteristics and properties. This is further confirmed by the similarity in thermal stability, antibacterial, and biological results obtained from both.

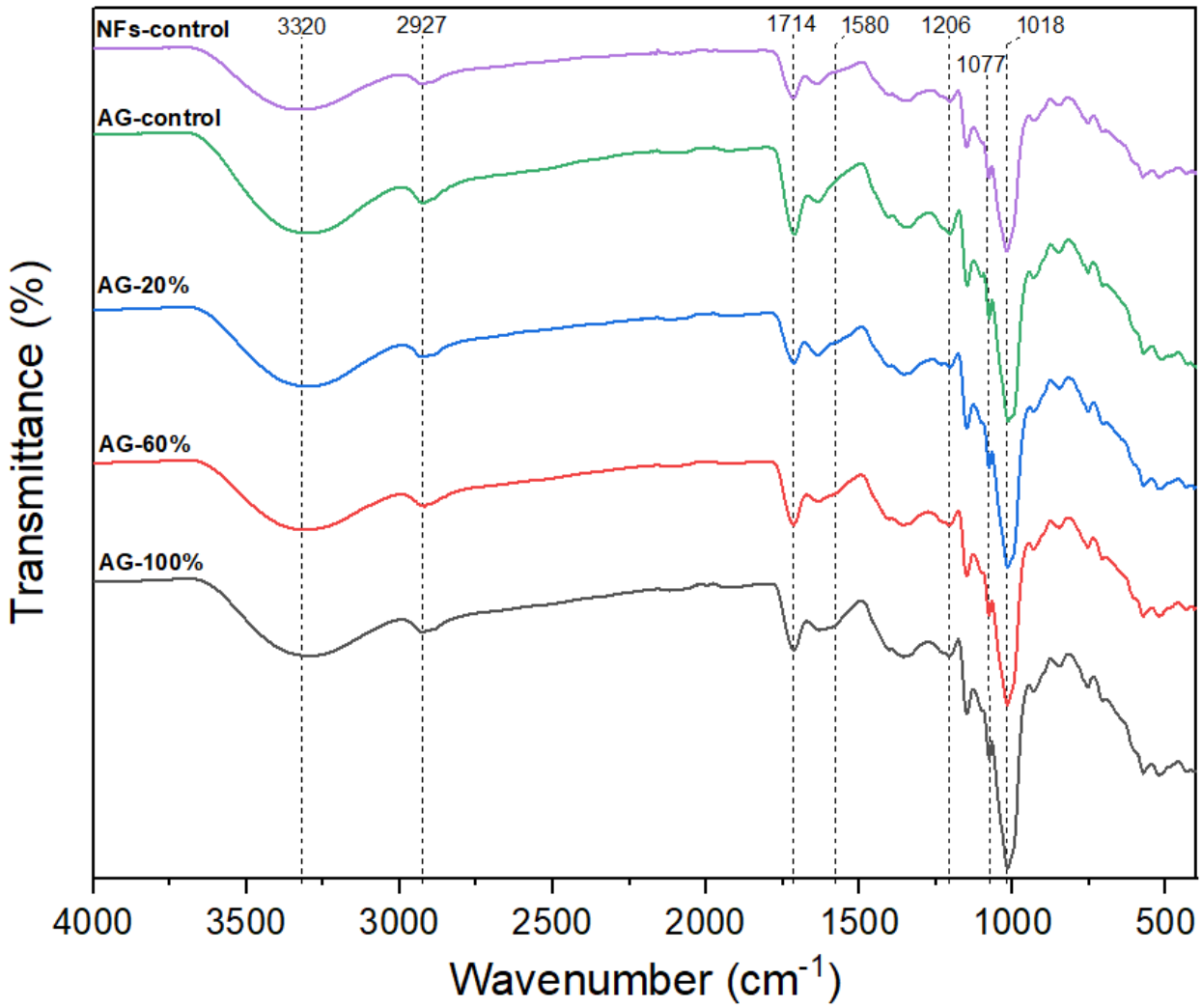

Figure 29. FTIR spectrum of the cross-linked composite NF control sample, AG-control, AG-20%, AG-60%, and AG-100%.

CHAPTER VI

CONCLUSION

6.1 Conclusion

Biocompatible fiber-based composite aerogels with synergistic antibacterial activity against E. coli and capability to promote cell attachment and growth were successfully produced from NFs via Forcespinning®. The aerogels produced were made from natural biocompatible, biodegradable products which included PL, CS, CA, and AVE. Cell culture and in vitro cell process illustrates that the developed antibacterial composite samples are non-cytotoxic to NIH 3T3 fibroblast cells and effectively advocate fibroblast cells attachment, as well as interlayer cells growth. Its porous 3D structure makes it a potential candidate for wound dressing application that will allow wounds to breath, absorbed excessive blood and exudates, and provide protection from infections while displaying good thermal stability.

The method in this study could be suitable to produce different NF-based aerogels from other materials to obtain similar physicochemical properties for wound dressing or a wide range of other applications. This study contributed to develop an understanding of the creation of fiber-based composite aerogels from biocompatible materials using Forcespinning® technology.

REFERENCES

[1] Orgill, Dennis P., and Carlos Blanco, eds. Biomaterials for treating skin loss. Elsevier, 2009.

[2] Stacey, M. "Why don't wounds heal." Wounds International 7.1 (2016): 16-21.

[3] Guo, S. al, and Luisa A. DiPietro. "Factors affecting wound healing." Journal of dental research 89.3 (2010): 219-229.

[4] Versteeg, Henri H., et al. "New fundamentals in hemostasis." Physiological reviews 93.1 (2013): 327-358.

[5] Bielefeld, Kirsten A., Saeid Amini-Nik, and Benjamin A. Alman. "Cutaneous wound healing: recruiting developmental pathways for regeneration." Cellular and Molecular Life Sciences 70.12 (2013): 2059-2081.

[6] Rajendran, Naresh Kumar, et al. "A review on nanoparticle based treatment for wound healing." Journal of Drug Delivery Science and Technology 44 (2018): 421-430.

[7] Delavary, Babak Mahdavian, et al. "Macrophages in skin injury and repair." Immunobiology 216.7 (2011): 753-762.

[8] Wynn, Thomas A., and Luke Barron. "Macrophages: master regulators of inflammation and fibrosis." Seminars in liver disease. Vol. 30. No. 3. NIH Public Access, 2010.

[9] Kendall, Ryan T., and Carol A. Feghali-Bostwick. "Fibroblasts in fibrosis: novel roles and mediators." Frontiers in pharmacology 5 (2014): 123.

[10] Zhang, Qiangqiang, et al. "Flyweight 3D graphene scaffolds with microinterface barrier-derived tunable thermal insulation and flame retardancy." ACS applied materials & interfaces 9.16 (2017): 14232-14241.

[11] Zu, Guoqing, et al. "Versatile double-cross-linking approach to transparent, machinable, supercompressible, highly bendable aerogel thermal superinsulators." Chemistry of Materials 30.8 (2018): 2759-2770.

[12] Cai, Huafei, et al. "Preparation of silica aerogels with high temperature resistance and low thermal conductivity by monodispersed silica sol." Materials & Design (2020): 108640.

[13] Regan, M. C., and A. Barbul. "The cellular biology of wound healing." Wound healing 1 (1994): 3-17.

[14] Healing, Wound. "Methods and Protocols." Methods in Molecular Medicine, LA DiPietro, AL Burns, Eds., Humana Press, Totowa, NJ (2003).

[15] Witte, Maria B., and Adrian Barbul. "Role of nitric oxide in wound repair." The American Journal of Surgery 183.4 (2002): 406-412.

[16] Lorenz, H. Peter, and Michael T. Longaker. "Wounds: biology, pathology, and management." Essential Practice of Surgery. Springer, New York, NY, 2003. 77-88.

[17] Dealey, Carol. The care of wounds: A guide for nurses. John Wiley & Sons, 2008.

[18] Martin, Paul. "Wound healing--aiming for perfect skin regeneration." Science 276.5309 (1997): 75-81.

[19] Gurtner, Geoffrey C., et al. "Wound repair and regeneration." Nature 453.7193 (2008): 314-321.

[20] Meyers, Lydia, S. L. Hudson, and Just Learning. "Wound Care: Getting to the Depth of the Tissue." Lakeway Texas: The National Center of Continuing Education (2013): 1-16.

[21] Järbrink, Krister, et al. "Prevalence and incidence of chronic wounds and related complications: a protocol for a systematic review." Systematic reviews 5.1 (2016): 152.

[22] Topical application of bacteriophages for treatment of wound infections

[23] Kordestani, Soheila S. Atlas of Wound Healing-E-Book: A Tissue Engineering Approach. Elsevier, 2019.

[24] Keyes, Brice E., et al. "Impaired epidermal to dendritic T cell signaling slows wound repair in aged skin." Cell 167.5 (2016): 1323-1338.

[25] Quain, Angela M., and Nancy M. Khardori. "Nutrition in Wound Care Management: A Comprehensive Overview." Wounds: a compendium of clinical research and practice 27.12 (2015): 327-335.

[26] Frykberg, Robert G., and Jaminelli Banks. "Challenges in the treatment of chronic wounds." Advances in wound care 4.9 (2015): 560-582.

[27] Reiber, Gayle E., et al. "Causal pathways for incident lower-extremity ulcers in patients with diabetes from two settings." Diabetes care 22.1 (1999): 157-162.

[28] Frykberg, Robert G., et al. "A multinational, multicenter, randomized, double-blinded, placebo-controlled trial to evaluate the efficacy of cyclical topical wound oxygen (TWO2) therapy in the treatment of chronic diabetic foot ulcers: the TWO2 study." Diabetes Care 43.3 (2020): 616-624.

[29] Brownrigg, J. R. W., et al. "Evidence-based management of PAD & the diabetic foot." European Journal of Vascular and Endovascular Surgery 45.6 (2013): 673-681.

[30] Singh, Nalini, David G. Armstrong, and Benjamin A. Lipsky. "Preventing foot ulcers in patients with diabetes." Jama 293.2 (2005): 217-228.

[31] Frykberg, Robert G., et al. "Diabetic foot disorders: a clinical practice guideline (2006 revision)." The journal of foot and ankle surgery 45.5 (2006): S1-S66.

[32] Boulton, Andrew JM, et al. "The global burden of diabetic foot disease." The Lancet 366.9498 (2005): 1719-1724.

[33] Moulik, Probal K., Robert Mtonga, and Geoffrey V. Gill. "Amputation and mortality in new-onset diabetic foot ulcers stratified by etiology." Diabetes care 26.2 (2003): 491-494.

[34] Jeffcoate, William J., et al. "Current challenges and opportunities in the prevention and management of diabetic foot ulcers." Diabetes care 41.4 (2018): 645-652.

[35] Iversen, Marjolein M., et al. "History of foot ulcer increases mortality among individuals with diabetes: ten-year follow-up of the Nord-Trøndelag Health Study, Norway." Diabetes care 32.12 (2009): 2193-2199.

[36] Brennan, Meghan B., et al. "Diabetic foot ulcer severity predicts mortality among veterans with type 2 diabetes." Journal of diabetes and its complications 31.3 (2017): 556-561.

[37] Morbach, Stephan, et al. "Long-term prognosis of diabetic foot patients and their limbs: amputation and death over the course of a decade." Diabetes care 35.10 (2012): 2021-2027.

[38] Armstrong, David G., James Wrobel, and Jeffery M. Robbins. "Guest editorial: are diabetes-related wounds and amputations worse than cancer." Int Wound J 4.4 (2007): 286-287.

[39] Nabuurs-Franssen, M. H., et al. "Health-related quality of life of diabetic foot ulcer patients and their caregivers." Diabetologia 48.9 (2005): 1906-1910.

[40] Rice, J. Bradford, et al. "Burden of diabetic foot ulcers for medicare and private insurers." Diabetes care 37.3 (2014): 651-658.

[41] Ragnarson Tennvall, Gunnel, and Jan Apelqvist. "Health-economic consequences of diabetic foot lesions." Clinical Infectious Diseases 39. Supplement_2 (2004): S132-S139.

[42] Grey, Joseph E., and Stuart Enoch. "ABC of wound healing: pressure ulcers." BMJ 332.Suppl S6 (2006).

[43] Al Aboud, Ahmad M. and Biagio Manna . “Wound Pressure Injury Management.” StatPearls, StatPearls Publishing, 28 June 2020.

[44] Kirman, C. N. "Pressure injuries (Pressure Ulcers) and wound care." Medscape J Med (2018).

[45] National Pressure Ulcer Advisory Panel. "NPUAP pressure injury stages." (2016).

[46] Shahin, Eman SM, Theo Dassen, and Ruud JG Halfens. "Pressure ulcer prevalence and incidence in intensive care patients: a literature review." Nursing in critical care 13.2 (2008): 71-79.

[47] Tubaishat, Ahmad, et al. "Pressure ulcers prevalence in the acute care setting: a systematic review, 2000-2015." Clinical nursing research 27.6 (2018): 643-659.

[48] Shahin, Eman SM, Theo Dassen, and Ruud JG Halfens. "Pressure ulcer prevalence in intensive care patients: a cross-sectional study." Journal of evaluation in clinical practice 14.4 (2008): 563-568.

[49] Pender, Lauren R., and Susan K. Frazier. "The relationship between dermal pressure ulcers, oxygenation and perfusion in mechanically ventilated patients." Intensive and critical care nursing 21.1 (2005): 29-38.

[50] US Department of Health & Human Services, Agency for Healthcare Research and Quality. Are we ready for this change: Preventing pressure ulcers in hospitals—a toolkit for improving quality of care. http://www.ahrq.gov/professionals/systems/long-termcare/resources/pressure-ulcers/pressureulcertoolkit/putool1.html

[51] James, William D., et al. Andrews' Diseases of the Skin: Clinical Dermatology. 12th ed., Elsevier, 2006.

[52] Grey, Joseph E., Stuart Enoch, and Keith G. Harding. "ABC of wound healing: Venous and arterial leg ulcers." Bmj 332.Suppl S4 (2006).

[53] Rayner, Robyn, et al. "Leg ulcers: atypical presentations and associated comorbidities." Wound Practice and Research 17.4 (2009): 168-185.

[54] Valencia, Isabel C., et al. "Chronic venous insufficiency and venous leg ulceration." Journal of the American Academy of Dermatology 44.3 (2001): 401-424.

[55] Rice, J. Bradford, et al. "Burden of venous leg ulcers in the United States." Journal of medical economics 17.5 (2014): 347-356.

[56] Nelzen, O. "Leg ulcers: economic aspects." Phlebology 15.3-4 (2000): 110-114.

[57] Xie, X., M. McGregor, and N. Dendukuri. "The clinical effectiveness of negative pressure wound therapy: a systematic review." Journal of wound care 19.11 (2010): 490-495.

[58] Ubbink, Dirk T., et al. "Topical negative pressure for treating chronic wounds." Cochrane database of systematic reviews 1 (2001).

[59] Secretariat, Medical Advisory. "Negative Pressure Wound Therapy: An Evidence-Based Analysis." Ontario health technology assessment series 6.14 (2006): 1.

[60] Rhee, Susan M., et al. "Negative pressure wound therapy technologies for chronic wound care in the home setting: A systematic review." Wound Repair and Regeneration 23.4 (2015): 506-517.

[61] Kloth, Luther C. "How to use electrical stimulation for wound healing." Nursing2019 32.12 (2002): 17.

[62] Thakral, Gaurav, et al. "Electrical stimulation to accelerate wound healing." Diabetic foot & ankle 4.1 (2013): 22081.

[63] Ud-Din, Sara, and Ardeshir Bayat. "Electrical stimulation and cutaneous wound healing: a review of clinical evidence." Healthcare. Vol. 2. No. 4. Multidisciplinary Digital Publishing Institute, 2014.

[64] Ter Haar, Gail. "Therapeutic ultrasound." European Journal of ultrasound 9.1 (1999): 3-9.

[65] Rashidi, Samaneh. "A review of mechanism of actions of ultrasound waves for treatment of soft tissue injuries." International Journal of Green Pharmacy (IJGP) 11.01 (2017).

[66] Shankar, Hariharan, and Paul S. Pagel. "Potential adverse ultrasound-related biological effectsa critical review." Anesthesiology: The Journal of the American Society of Anesthesiologists 115.5 (2011): 1109-1124.

[67] Hess, Christopher L., Michael A. Howard, and Christopher E. Attinger. "A review of mechanical adjuncts in wound healing: hydrotherapy, ultrasound, negative pressure therapy, hyperbaric oxygen, and electrostimulation." Annals of plastic surgery 51.2 (2003): 210-218.

[68] Nigam, Yamni, et al. "Maggot therapy: the science and implication for CAM Part I—history and bacterial resistance." Evidence-based complementary and Alternative Medicine 3 (2006).

[69] Turkmen, Arif, Ken Graham, and D. A. McGrouther. "Therapeutic applications of the larvae for wound debridement." Journal of plastic, reconstructive & aesthetic surgery 63.1 (2010): 184-188.

[70] Schoukens, Gustaaf. "Bioactive dressings to promote wound healing." Advanced textiles for wound care. Woodhead Publishing, 2009. 114-152.

[71] Kordestani, Soheila S. Atlas of Wound Healing: A Tissue Engineering Approach. Elsevier, 2019. pp. 31-47.

[72] Abrigo, Martina, Sally L. McArthur, and Peter Kingshott. "Electrospun nanofibers as dressings for chronic wound care: advances, challenges, and future prospects." Macromolecular bioscience 14.6 (2014): 772-792.

[73] Xu, Fenghua, et al. "Large-scale production of a ternary composite nanofiber membrane for wound dressing applications." Journal of bioactive and compatible polymers 29.6 (2014): 646-660.

[74] Akia, Mandana, et al. "Texas Sour Orange Juice Used in Scaffolds for Tissue Engineering." Membranes 8.3 (2018): 38.

[75] Sarhan, Wessam A., Hassan ME Azzazy, and Ibrahim M. El-Sherbiny. "Honey/chitosan nanofiber wound dressing enriched with Allium sativum and Cleome droserifolia: enhanced antimicrobial and wound healing activity." ACS applied materials & interfaces 8.10 (2016): 6379-6390.

[76] Kistler, Samuel Stephens. "Coherent expanded aerogels and jellies." Nature 127.3211 (1931): 741-741.

[77] Pierre, Alain C., and Gerard M. Pajonk. "Chemistry of aerogels and their applications." Chemical Reviews 102.11 (2002): 4243-4266.

[78] Ziegler, Christoph, et al. "Modern inorganic aerogels." Angewandte Chemie International Edition 56.43 (2017): 13200-13221.

[79] Zhao, Shanyu, et al. "Biopolymer aerogels and foams: Chemistry, properties, and applications." Angewandte Chemie International Edition 57.26 (2018): 7580-7608.

[80] Budtova, Tatiana. "Cellulose II aerogels: A review." Cellulose 26.1 (2019): 81-121.

[81] Sun, Haiyan, Zhen Xu, and Chao Gao. "Multifunctional, ultra-flyweight, synergistically assembled carbon aerogels." Advanced Materials 25.18 (2013): 2554-2560.

[82] Hu, Han, et al. "Ultralight and highly compressible graphene aerogels." Advanced materials 25.15 (2013): 2219-2223

[83] Liang, Hai-Wei, et al. "Macroscopic-scale template synthesis of robust carbonaceous nanofiber hydrogels and aerogels and their applications." Angewandte Chemie International Edition 51.21 (2012): 5101-5105.

[84] Schaedler, Tobias A., et al. "Ultralight metallic microlattices." Science 334.6058 (2011): 962-965.

[85] Zhang, Qiangqiang, et al. "Flyweight 3D graphene scaffolds with microinterface barrier-derived tunable thermal insulation and flame retardancy." ACS Applied Materials & Interfaces 9.16 (2017): 14232-14241.

[86] Zu, Guoqing, et al. "Versatile double-cross-linking approach to transparent, machinable, supercompressible, highly bendable aerogel thermal superinsulators." Chemistry of Materials 30.8 (2018): 2759-2770.

[87] Cai, Huafei, et al. "Preparation of silica aerogels with high temperature resistance and low thermal conductivity by monodispersed silica sol." Materials & Design (2020): 108640.

[88] Wong, Joanna CH, et al. "Mechanical properties of monolithic silica aerogels made from polyethoxydisiloxanes." Microporous and mesoporous materials 183 (2014): 23-29.

[89] Cai, Jie, et al. "Cellulose aerogels from aqueous alkali hydroxide–urea solution." ChemSusChem 1.1-2 (2008): 149-154.

[90] Sehaqui, Houssine, Qi Zhou, and Lars A. Berglund. "High-porosity aerogels of high specific surface area prepared from nanofibrillated cellulose (NFC)." Composites science and technology 71.13 (2011): 1593-1599.

[91] Hüsing, Nicola, and Ulrich Schubert. "Aerogels—airy materials: chemistry, structure, and properties." Angewandte Chemie International Edition 37.1-2 (1998): 22-45.

[92] Lu, Tianhong, et al. "Composite aerogels based on dialdehyde nanocellulose and collagen for potential applications as wound dressing and tissue engineering scaffold." Composites Science and Technology 94 (2014): 132-138.

[93] Green Fabrication of Amphiphilic Quaternized β-Chitin Derivatives with Excellent Biocompatibility and Antibacterial Activities for Wound Healing

[94] Maleki, Hajar, et al. "Mechanically strong silica-silk fibroin bioaerogel: a hybrid scaffold with ordered honeycomb micromorphology and multiscale porosity for bone regeneration." ACS applied materials & interfaces 11.19 (2019): 17256-17269

[95] Zhang, Jintao, Zhenhai Xia, and Liming Dai. "Carbon-based electrocatalysts for advanced energy conversion and storage." Science advances 1.7 (2015): e1500564.

[96] Worsley, Marcus A., et al. "Synthesis of graphene aerogel with high electrical conductivity." Journal of the American Chemical Society 132.40 (2010): 14067-14069.

[97] Kistler, Samuel S. "Coherent expanded-aerogels." The Journal of Physical Chemistry 36.1 (2002): 52-64.

[98] Teichner, S. J., et al. "Inorganic oxide aerogels." Advances in Colloid and Interface Science 5.3 (1976): 245-273.

[99] Ülker, Zeynep, Deniz Sanli, and Can Erkey. "Applications of aerogels and their composites in energy-related technologies." Supercritical fluid technology for energy and environmental applications. Elsevier, 2014. 157-180.

[100] Hench, Larry L., and Jon K. West. "The sol-gel process." Chemical reviews 90.1 (1990): 33-72.

[101] Pillai, Suresh C., and Sarah Hehir, eds. Sol-gel materials for energy, environment and electronic applications. New York: Springer, 2017.

[102] Dorcheh, A. Soleimani, and M. H. Abbasi. "Silica aerogel; synthesis, properties and characterization." Journal of materials processing technology 199.1-3 (2008): 10-26.

[103] Pierre, Alain C., and Gerard M. Pajonk. "Chemistry of aerogels and their applications." Chemical Reviews 102.11 (2002): 4243-4266.

[104] Unlusu, Betul, Sermin G. Sunol, and Aydin K. Sunol. "Stress formation during heating in supercritical drying." Journal of non-crystalline solids 279.2-3 (2001): 110-118.

[105] Woignier, Thierry, George W. Scherer, and Adil Alaoui. "Stress in aerogel during depressurization of autoclave: II. Silica gels." Journal of Sol-Gel Science and Technology 3.2 (1994): 141-150.

[106] Aravind, P. R., et al. "Ambient pressure drying: a successful approach for the preparation of silica and silica based mixed oxide aerogels." Journal of sol-gel science and technology 54.1 (2010): 105-117.

[107] Han, Xiao, et al. "Bioinspired synthesis of monolithic and layered aerogels." Advanced Materials 30.23 (2018): 1706294.

[108] Deuber, Fabian, and Christian Adlhart. "From short electrospun nanofibers to ultralight aerogels with tunable pore structure." CHIMIA International Journal for Chemistry 71.4 (2017): 236-240.

[109] Schiraldi, David A. "Green Polymer Aerogels." Green Polymer Chemistry: Biobased Materials and Biocatalysis. American Chemical Society, 2015. 471-482.

[110] Si, Yang, et al. "Ultralight nanofibre-assembled cellular aerogels with superelasticity and multifunctionality." Nature communications 5.1 (2014): 1-9.

[111] Ewulonu, Chinomso M., et al. "Fabrication of cellulose nanofiber/polypyrrole/polyvinylpyrrolidone aerogels with box-Behnken design for optimal electrical conductivity." Carbohydrate Polymers 235 (2020): 116028.

[112] Deuber, Fabian, et al. "Exploration of ultralight nanofiber aerogels as particle filters: capacity and efficiency." ACS applied materials & interfaces 10.10 (2018): 9069-9076.

[113] Huang, Yunpeng, et al. "Elastic carbon aerogels reconstructed from electrospun nanofibers and graphene as three-dimensional networked matrix for efficient energy storage/conversion." Scientific reports 6.1 (2016): 1-11. [114]

[114] Si, Yang, et al. "Superelastic and superhydrophobic nanofiber-assembled cellular aerogels for effective separation of oil/water emulsions." ACS nano 9.4 (2015): 3791-3799.

[115] Xu, Tao, et al. "Three-dimensional monolithic porous structures assembled from fragmented electrospun nanofiber mats/membranes: Methods, properties, and applications." Progress in Materials Science (2020): 100656.

[116] Armor, J. N., E. J. Carlson, and P. M. Zambri. "Aerogels as hydrogenation catalysts." Applied catalysis 19.2 (1985): 339-348.

[117] Mizushima, Yasuyuki, and Makoto Hori. "Properties of alumina aerogels prepared under different conditions." Journal of non-crystalline solids 167.1-2 (1994): 1-8.

[118] Dutoit, D. C. M., M. Schneider, and A. Baiker. "Titania-silica mixed oxides. I. Influence of sol-gel and drying conditions on structural properties." Journal of Catalysis 153.1 (1995): 165-176.

[119] Chaput, F., et al. "Synthesis and characterization of vanadium oxide aerogels." Journal of non-crystalline solids 188.1-2 (1995): 11-18.

[120] Suh, Dong Jin, and Tae-Jin Park. "Sol− gel strategies for pore size control of high-surface-area transition-metal oxide aerogels." Chemistry of materials 8.2 (1996): 509-513.

[121] Pekala, R. W. "Organic aerogels from the polycondensation of resorcinol with formaldehyde." Journal of materials science 24.9 (1989): 3221-3227.

[122] Grishechko, L. I., et al. "New tannin–lignin aerogels." Industrial Crops and Products 41 (2013): 347-355.

[123] Pekala, R. W., C. T. Alviso, and J. D. LeMay. "Organic aerogels: microstructural dependence of mechanical properties in compression." Journal of non-crystalline solids 125.1-2 (1990): 67-75.

[124] Szczurek, A., et al. "The use of tannin to prepare carbon gels. Part I: Carbon aerogels." Carbon 49.8 (2011): 2773-2784.

[125] Wu, Zhong-Shuai, et al. "3D nitrogen-doped graphene aerogel-supported Fe3O4 nanoparticles as efficient electrocatalysts for the oxygen reduction reaction." Journal of the American Chemical Society 134.22 (2012): 9082-9085.

[126] Wu, Zhong-Shuai, et al. "Three-dimensional graphene-based macro-and mesoporous frameworks for high-performance electrochemical capacitive energy storage." Journal of the American Chemical Society 134.48 (2012): 19532-19535.

[127] Olsson, Richard T., et al. "Making flexible magnetic aerogels and stiff magnetic nanopaper using cellulose nanofibrils as templates." Nature nanotechnology 5.8 (2010): 584-588.

[128] Xiao, Li, et al. "Self-assembled Fe2O3/graphene aerogel with high lithium storage performance." ACS applied materials & interfaces 5.9 (2013): 3764-3769.

[129] Yao, Qiufang, et al. "3D assembly based on 2D structure of cellulose nanofibril/graphene oxide hybrid aerogel for adsorptive removal of antibiotics in water." Scientific reports 7 (2017): 45914.

[130] Xu, Xiang, et al. "Self-sensing, ultralight, and conductive 3D graphene/iron oxide aerogel elastomer deformable in a magnetic field." ACS nano 9.4 (2015): 3969-3977.

[131] Lesnyak, Vladimir, et al. "3D assembly of semiconductor and metal nanocrystals: hybrid CdTe/Au structures with controlled content." Journal of the American Chemical Society 133.34 (2011): 13413-13420.

[132] Zeng, Guobo, et al. "A general method of fabricating flexible spinel-type oxide/reduced graphene oxide nanocomposite aerogels as advanced anodes for lithium-ion batteries." ACS nano 9.4 (2015): 4227-4235.

[133] Moreno-Castilla, C., and F. J. Maldonado-Hódar. "Carbon aerogels for catalysis applications: An overview." Carbon 43.3 (2005): 455-465.

[134] Wang, Yixin, et al. "The advances of polysaccharide-based aerogels: Preparation and potential application." Carbohydrate polymers 226 (2019): 115242.

[135] Dumitriu, Severian, ed. Polysaccharides: structural diversity and functional versatility. CRC press, 2004.

[136] Yagoub, Hajo, et al. "Complex aerogels generated from nano-polysaccharides and its derivatives for oil–water separation." Polymers 11.10 (2019): 1593.

[137] Guo, Mark Q., et al. "Polysaccharides: structure and solubility." Solubility of polysaccharides (2017): 7-21.

[138] El-Naggar, Mehrez E., et al. "Synthesis, drying process and medical application of polysaccharide-based aerogels." International journal of biological macromolecules 145 (2020): 1115-1128.

[139] Zheng, Yingying, Jonathan Monty, and Robert J. Linhardt. "Polysaccharide-based nanocomposites and their applications." Carbohydrate research 405 (2015): 23-32.

[140] Sila, Assaâd, et al. "Water-soluble polysaccharides from agro-industrial by-products: functional and biological properties." International journal of biological macromolecules 69 (2014): 236-243.

[141] Ren, Yan, et al. "The preparation and structure analysis methods of natural polysaccharides of plants and fungi: A review of recent development." Molecules 24.17 (2019): 3122.

[142] Trinetta, V., and C. N. Cutter. "Pullulan: A suitable biopolymer for antimicrobial food packaging applications." Antimicrobial Food Packaging. Academic Press, 2016. 385-397.

[143] Abhilash, M., and D. Thomas. "Biopolymers for biocomposites and chemical sensor applications." Biopolymer Composites in Electronics. Elsevier, 2017. 405-435.

[144] Singh, Ram Sarup, Navpreet Kaur, and John F. Kennedy. "Pullulan and pullulan derivatives as promising biomolecules for drug and gene targeting." Carbohydrate Polymers 123 (2015): 190-207.

[145] Hasegawa, Urara, et al. "Nanogel-quantum dot hybrid nanoparticles for live cell imaging." Biochemical and biophysical research communications 331.4 (2005): 917-921.

[146] Popa, Valentin. Polysaccharides in medicinal and pharmaceutical applications. Smithers Rapra, 2011.

[147] Wong, Victor W., et al. "Engineered pullulan–collagen composite dermal hydrogels improve early cutaneous wound healing." Tissue engineering part A 17.5-6 (2011): 631-644.

[148] Li, Huanan, et al. "Superabsorbent polysaccharide hydrogels based on pullulan derivate as antibacterial release wound dressing." Journal of Biomedical Materials Research Part A 98.1 (2011): 31-39.

[149] Xu, Fenghua, et al. "Development of tannic acid/chitosan/pullulan composite nanofibers from aqueous solution for potential applications as wound dressing." Carbohydrate polymers 115 (2015): 16-24.

[150] “Classification: USDA PLANTS.” Classification | USDA PLANTS, plants.usda.gov/java/ClassificationServlet?source=profile.

[151] Surjushe, Amar, Resham Vasani, and D. G. Saple. "Aloe vera: a short review." Indian journal of dermatology 53.4 (2008): 163.

[152] Bozzi, A., et al. "Quality and authenticity of commercial aloe vera gel powders." Food chemistry 103.1 (2007): 22-30.

[153] Benzie, Iris FF, and Sissi Wachtel-Galor, eds. Herbal medicine: biomolecular and clinical aspects. CRC press, 2011.

[154] Maenthaisong, Ratree, et al. "The efficacy of aloe vera used for burn wound healing: a systematic review." burns 33.6 (2007): 713-718.

[155] Visuthikosol, V., et al. "Effect of aloe vera gel to healing of burn wound a clinical and histologic study." J Med Assoc Thai 78.8 (1995): 403-9.

[156] Syed, Tanweer A., et al. "Management of psoriasis with Aloe vera extract in a hydrophilic cream: a placebo-controlled, double-blind study." Tropical Medicine & International Health 1.4 (1996): 505-509.

[157] Fulton Jr, James E. "The stimulation of postdermabrasion wound healing with stabilized aloe vera gel-polyethylene oxide dressing." The Journal of dermatologic surgery and oncology 16.5 (1990): 460-467.

[158] Jithendra, Panneerselvam, et al. "Preparation and characterization of aloe vera blended collagen-chitosan composite scaffold for tissue engineering applications." ACS applied materials & interfaces 5.15 (2013): 7291-7298.

[159] Suganya, S., et al. "Aloe vera incorporated biomimetic nanofibrous scaffold: a regenerative approach for skin tissue engineering." Iranian Polymer Journal 23.3 (2014): 237-248.

[160] Ferro, Valerie A., et al. "In vitro susceptibilities of Shigella flexneri and Streptococcus pyogenes to inner gel of Aloe barbadensis Miller." Antimicrobial agents and chemotherapy 47.3 (2003): 1137-1139.

[161] Radha, Maharjan H., and Nampoothiri P. Laxmipriya. "Evaluation of biological properties and clinical effectiveness of Aloe vera: A systematic review." Journal of traditional and complementary medicine 5.1 (2015): 21-26.

[162] Zhang, Linna, and Ian R. Tizard. "Activation of a mouse macrophage cell line by acemannan: the major carbohydrate fraction from Aloe vera gel." Immunopharmacology 35.2 (1996): 119-128.

[163] Bradbury, Savile, and David C. Joy. “Scanning Electron Microscope.” Encyclopædia Britannica, Encyclopædia Britannica, Inc., 30 Oct. 2019, www.britannica.com/technology/scanning-electron-microscope.

[164] Athiban, Prakash P., et al. "Evaluation of antimicrobial efficacy of Aloe vera and its effectiveness in decontaminating gutta percha cones." Journal of conservative dentistry: JCD 15.3 (2012): 246.

[165] Pandey, Ruchi, and Avinash Mishra. "Antibacterial activities of crude extract of Aloe barbadensis to clinically isolated bacterial pathogens." Applied biochemistry and biotechnology 160.5 (2010): 1356-1361.

[166] Lawrence, Rubina, Priyanka Tripathi, and Ebenezer Jeyakumar. "Isolation, purification and evaluation of antibacterial agents from Aloe vera." Brazilian Journal of Microbiology 40.4 (2009): 906-915.

[167] Perry, Seth W., et al. "Mitochondrial membrane potential probes and the proton gradient: a practical usage guide." Biotechniques 50.2 (2011): 98-115.

[168] Geisler, Sven, et al. "PINK1/Parkin-mediated mitophagy is dependent on VDAC1 and p62/SQSTM1." Nature cell biology 12.2 (2010): 119-131.

[169] Hanafiah, Megat Ahmad Kamal Megat, et al. "Methylene blue adsorption on Aloe vera rind powder: Kinetics, Isotherm and Mechanisms." Nature Environment and Pollution Technology 17.4 (2018): 1055-1064.

[170] Pathak, Pranav D., Sachin A. Mandavgane, and Bhaskar D. Kulkarni. "Characterizing fruit and vegetable peels as bioadsorbents." Current Science (2016): 2114-2123.

[171] Lewandowska, Katarzyna. "Miscibility and thermal stability of poly (vinyl alcohol)/chitosan mixtures." Thermochimica Acta 493.1-2 (2009): 42-48.

[172] Solaberrieta, Ignacio, et al. "Encapsulation of Bioactive Compounds from Aloe Vera Agrowastes in Electrospun Poly (Ethylene Oxide) Nanofibers." Polymers 12.6 (2020): 1323.

[173] Wu, Jia, et al. "Preparation and characterization of pullulan–chitosan and pullulan–carboxymethyl chitosan blended films." Food Hydrocolloids 30.1 (2013): 82-91.

[174] Singh, R. S., and G. K. Saini. "Pullulan-hyperproducing color variant strain of Aureobasidium pullulans FB-1 newly isolated from phylloplane of Ficus sp." Bioresource technology 99.9 (2008): 3896-3899.

[175] Tong, Qunyi, Qian Xiao, and Loong-Tak Lim. "Preparation and properties of pullulan–alginate–carboxymethylcellulose blend films." Food Research International 41.10 (2008): 1007-1014.

[176] Shingel, Kirill I. "Determination of structural peculiarities of dexran, pullulan and γ-irradiated pullulan by Fourier-transform IR spectroscopy." Carbohydrate Research 337.16 (2002): 1445-1451.

[177] Xu, Y. X., et al. "Chitosan–starch composite film: preparation and characterization." Industrial crops and Products 21.2 (2005): 185-192.

[178] Fernandes Queiroz, Moacir, et al. "Does the use of chitosan contribute to oxalate kidney stone formation?." Marine drugs 13.1 (2015): 141-158.

[179] Wang, Qun, et al. "Controlled release of ciprofloxacin hydrochloride from chitosan/polyethylene glycol blend films." Carbohydrate polymers 69.2 (2007): 336-343.

[180] He, Guanghua, et al. "Synthesis, characterization and antibacterial activity of salicyloyl chitosan." Carbohydrate polymers 83.3 (2011): 1274-1278.

[181] Shi, Rui, et al. "The effect of citric acid on the structural properties and cytotoxicity of the polyvinyl alcohol/starch films when molding at high temperature." Carbohydrate polymers 74.4 (2008): 763-770.

[182] Cheng, Kuan-Chen, Ali Demirci, and Jeffrey M. Catchmark. "Effects of plastic composite support and pH profiles on pullulan production in a biofilm reactor." Applied microbiology and biotechnology 86.3 (2010): 853-861.

[183] Abbasi, Muhammad SA, Muhammad Aslam Tahir, and Sidra Meer. "FTIR Spectroscopic study of aloe vera barbadensis Mill Buds." Asian Journal of Chemical Sciences (2020): 1-6.

[184] Lim, Zhe Xi, and Kuan Yew Cheong. "Effects of drying temperature and ethanol concentration on bipolar switching characteristics of natural Aloe vera-based memory devices." Physical Chemistry Chemical Physics 17.40 (2015): 26833-26853.

[185] Jithendra, Panneerselvam, et al. "Preparation and characterization of aloe vera blended collagen-chitosan composite scaffold for tissue engineering applications." ACS applied materials & interfaces 5.15 (2013): 7291-7298.

[186] Torres-Giner, Sergio, et al. "Nanoencapsulation of Aloe vera in synthetic and naturally occurring polymers by electrohydrodynamic processing of interest in food technology and bioactive packaging." Journal of Agricultural and Food Chemistry 65.22 (2017): 4439-4448.

[187] Li, Zongjie, et al. "Preparation and characterization of long-term stable pullulan nanofibers via in situ cross-linking electrospinning." Adsorption Science & Technology 37.5-6 (2019): 401-411.

[188] Deuber, Fabian, et al. "Exploration of ultralight nanofiber aerogels as particle filters: capacity and efficiency." ACS applied materials & interfaces 10.10 (2018): 9069-9076.

APPENDIX A

APPENDIX A

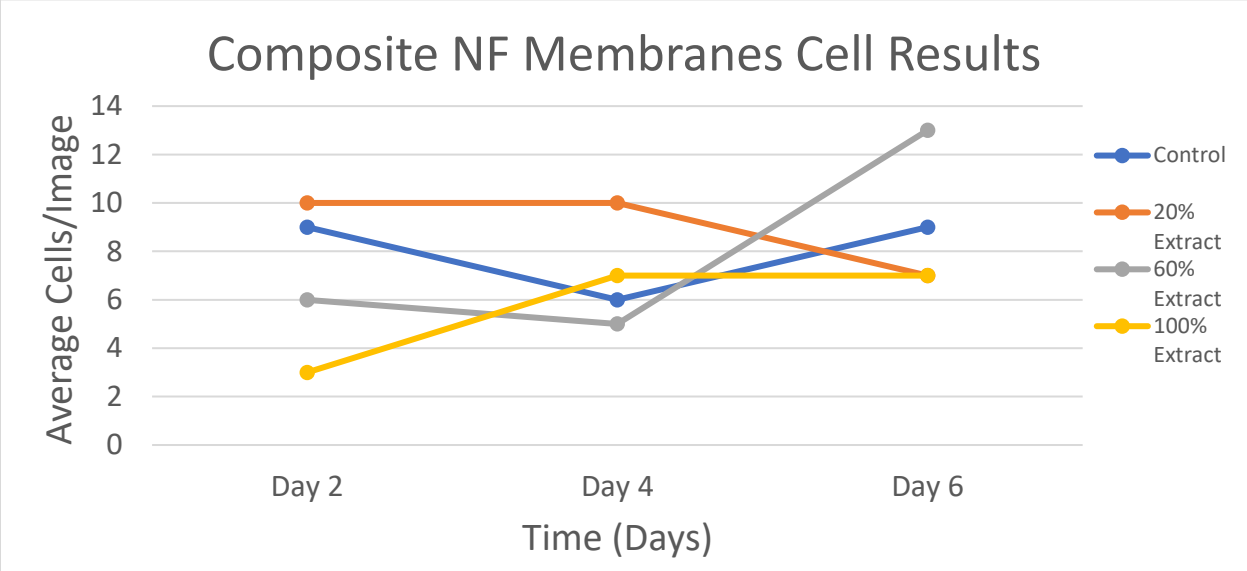

Figure A1 – Comparison of cell proliferation results from a 3-trial experiment for samples: control, 20% extract, 60% extract, and 100% extract.

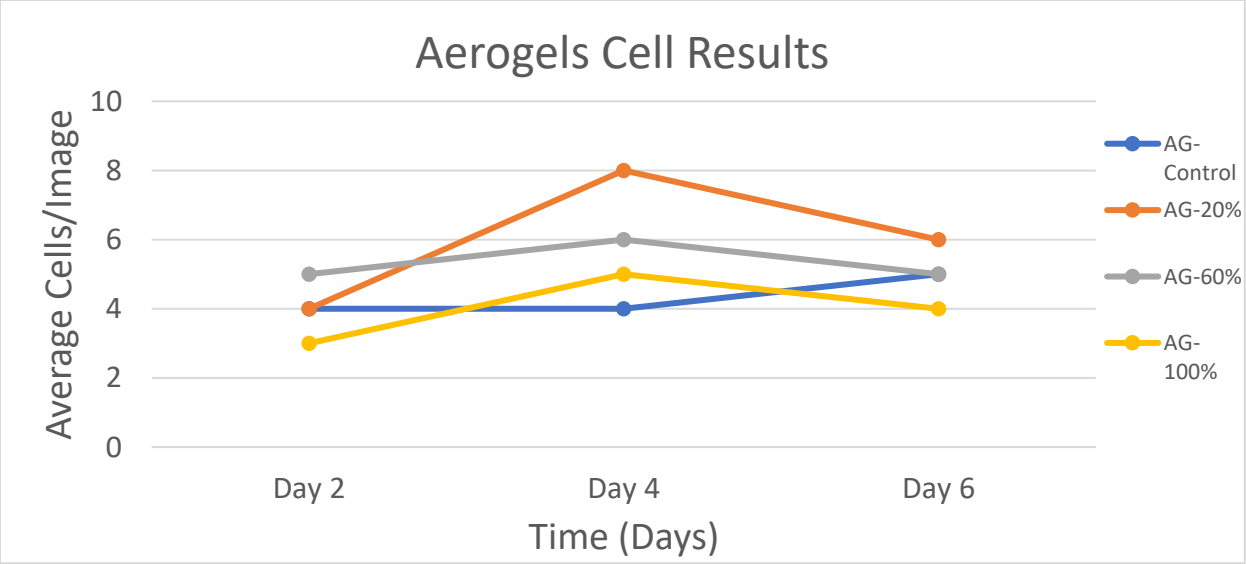

Figure A2 – Comparison of cell proliferation results from a 3-trial experiment for samples: AG-control, AG-20%, AG-60%, and AG-100%.

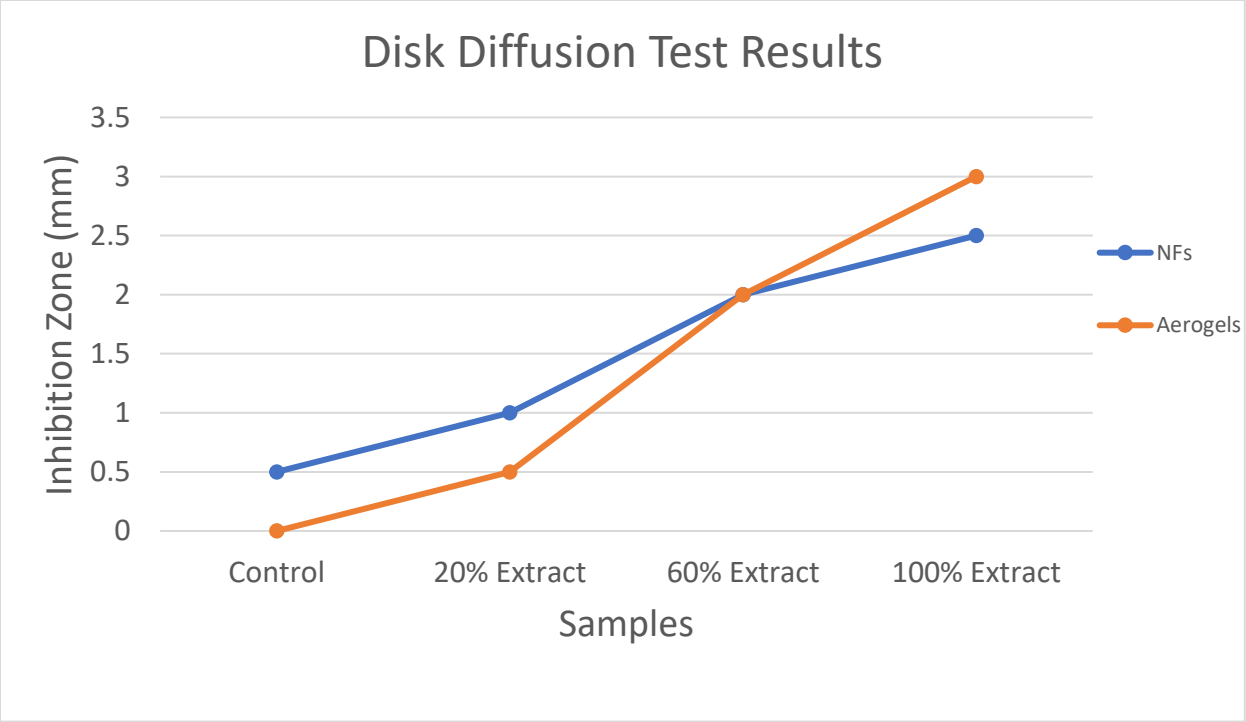

Figure A3 – Disk diffusion test results comparison between NFs membrane and aerogels.

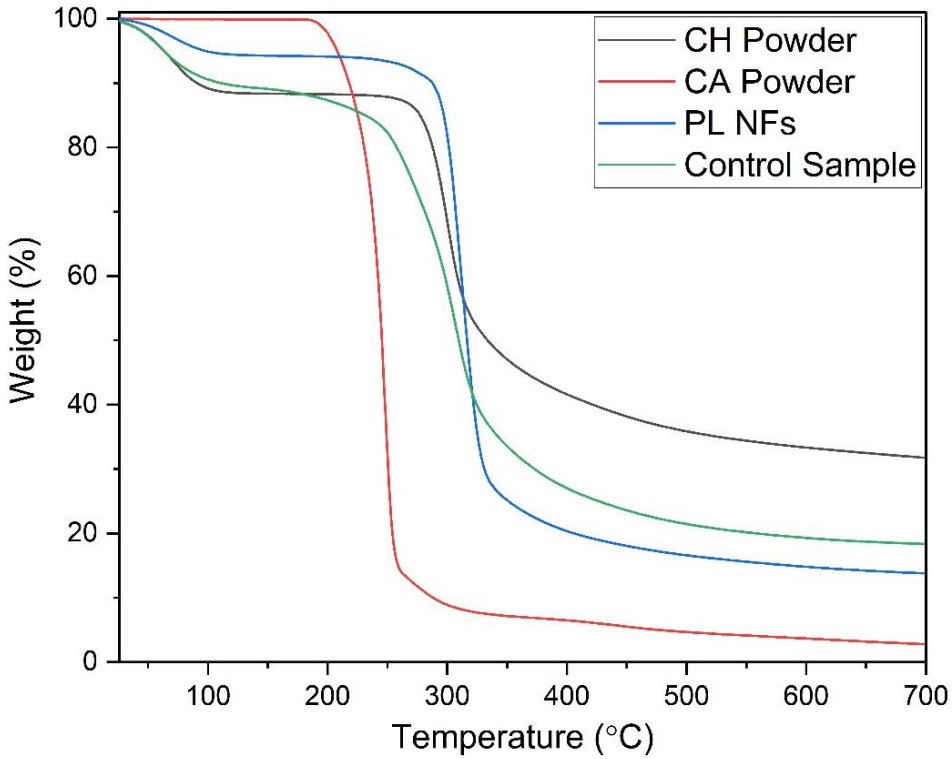

Figure A4. TGA curves of the control sample and the individual components that make up the composite NF membrane.

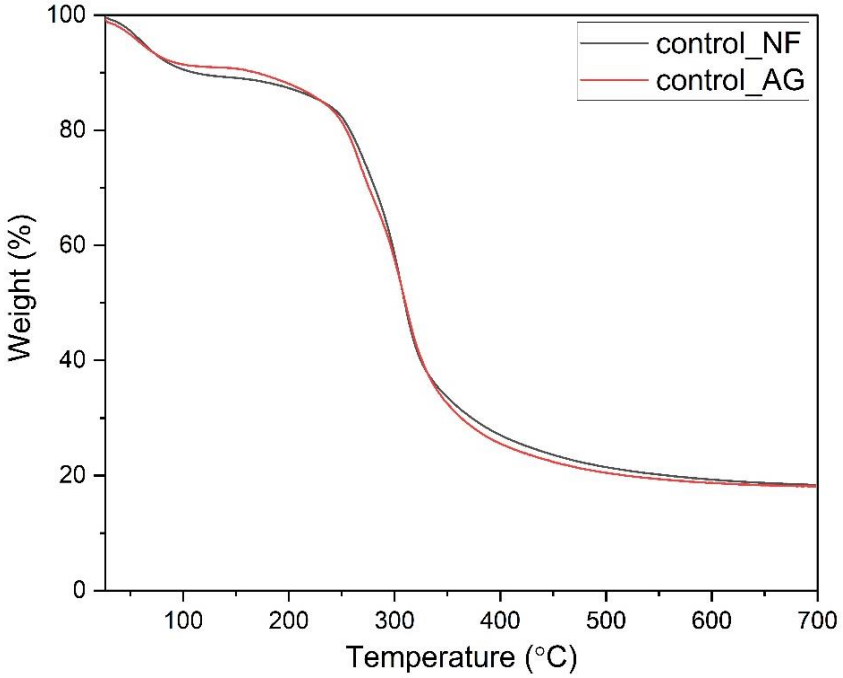

Figure A5. TGA curves comparing the control samples from the composite NF membrane and aerogel.

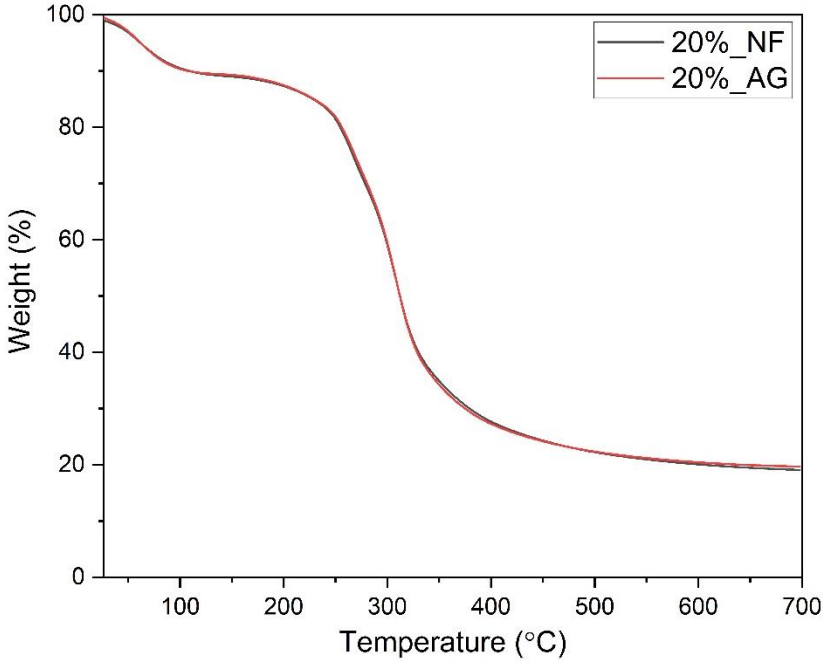

Figure A6. TGA curves comparing the 20% extracts samples from the composite NF membrane and aerogel.

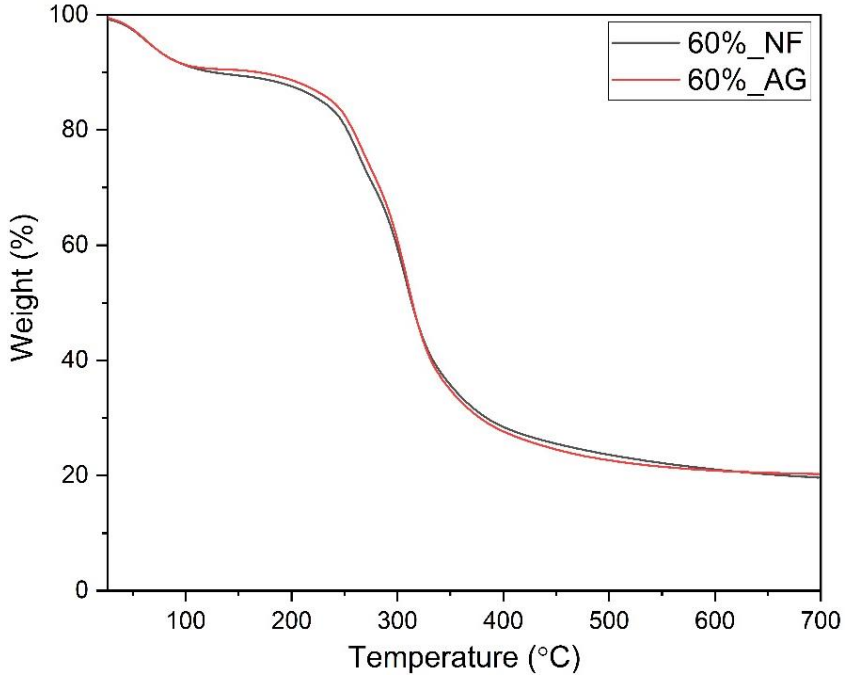

Figure A7. TGA curves comparing the 60% extracts samples from the composite NF membrane and aerogel.

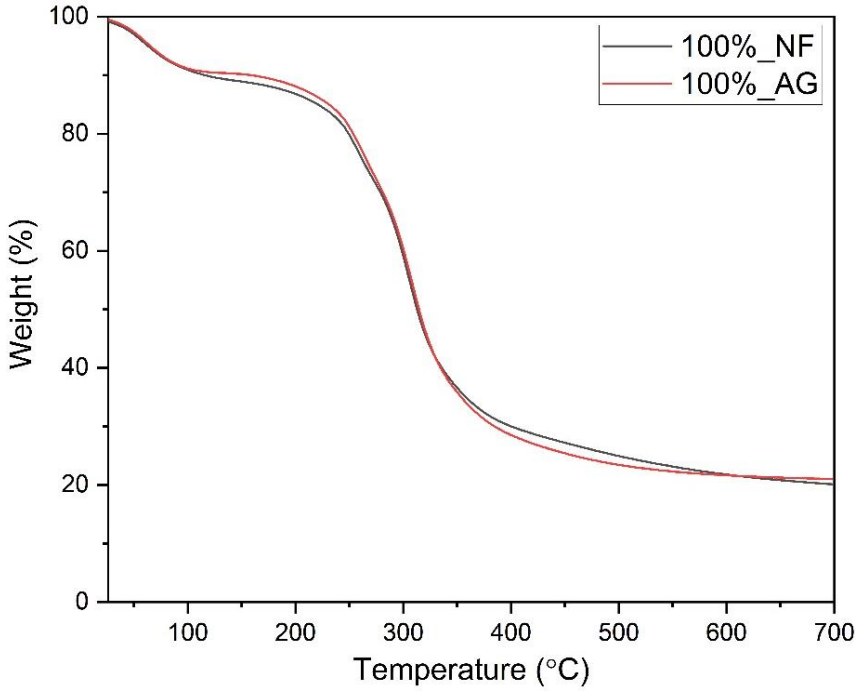

Figure A8. TGA curves comparing the 100% extracts samples for the composite NF membrane and aerogel.

BIOGRAPHICAL SKETCH

Raul C. Barbosa was born in Reynosa, Tamaulipas, Mexico. He completed elementary school in Mexico and then moved to the United States where he attended The Teacher's Academy and The Science Academy of South Texas for his middle and high school education.

Soon after, he attended The University of Texas Rio Grande Valley, where he graduated in May 2018 with a dual degree in Mechanical Engineering and Accounting. Subsequently, he was accepted to the Mechanical Engineering Graduate Program at the University of Texas Rio Grande Valley where he began working as a Graduate Research Assistant for Dr. Karen Lozano. During that time, he worked on multiple projects which included electromagnetic interference (EMI) shielding, production of graphene via polymer carbonization, wettability analysis, photoluminescent materials, construction of a portable Forcespinning® machine, and production of nanofiber-based aerogels.

He obtained his master's degree in August 2020 and is continuing his doctoral studies at The University of Texas at Austin in the Materials Science and Engineering program. His personal email is raul.barbosa@live.com.